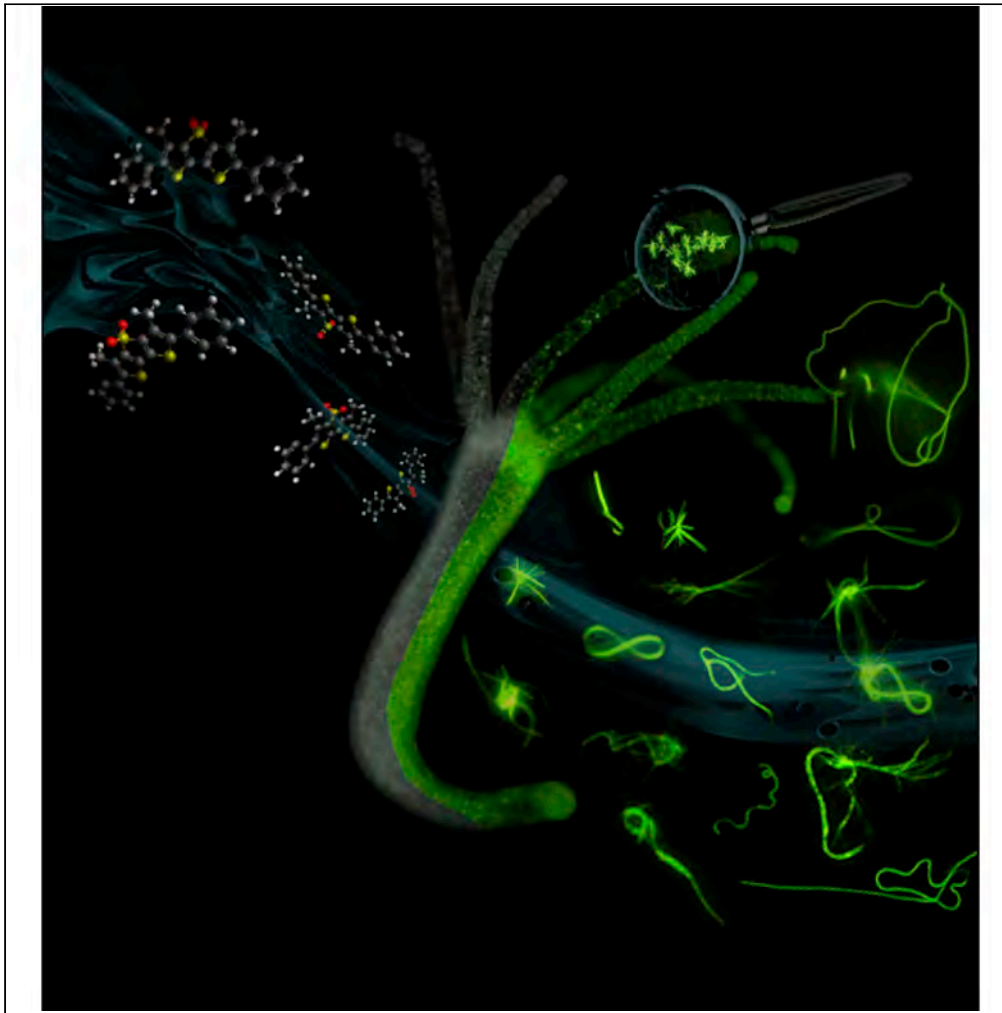


## Article

# In Vivo Bioengineering of Fluorescent Conductive Protein-Dye Microfibers



Maria Moros,  
Francesca Di  
Maria, Principia  
Dardano, ...,  
Angela Tino,  
Giovanna  
Barbarella,  
Claudia  
Tortiglione

claudia.tortiglione@cnr.it

**HIGHLIGHTS**

The oligothiophene DTTO promotes the synthesis of microfibers in *Hydra vulgaris*

DTTO co-assembles with proteins giving rise to fluorescent and conductive microfibers

The biofiber synthesis is an active process, based on protein synthesis

*In situ* produced hybrid microfibers have great potential in bioelectronics and biomedicine

Moros et al., iScience 23,  
101022  
April 24, 2020 © 2020 The  
Authors.  
[https://doi.org/10.1016/  
j.isci.2020.101022](https://doi.org/10.1016/j.isci.2020.101022)

## Article

# In Vivo Bioengineering of Fluorescent Conductive Protein-Dye Microfibers

Maria Moros,<sup>1,6</sup> Francesca Di Maria,<sup>2,3</sup> Principia Dardano,<sup>4,7</sup> Giuseppina Tommasini,<sup>1</sup> Hiram Castillo-Michel,<sup>5</sup> Alessandro Kovtun,<sup>2</sup> Mattia Zangoli,<sup>2</sup> Martina Blasio,<sup>1</sup> Luca De Stefano,<sup>4,7</sup> Angela Tino,<sup>1</sup> Giovanna Barbarella,<sup>2</sup> and Claudia Tortiglione<sup>1,8,\*</sup>

## SUMMARY

**Engineering protein-based biomaterials is extremely challenging in bioelectronics, medicine, and materials science, as mechanical, electrical, and optical properties need to be merged to biocompatibility and resistance to biodegradation. An effective strategy is the engineering of physiological processes *in situ*, by addition of new properties to endogenous components. Here we show that a green fluorescent semiconducting thiophene dye, DTTO, promotes, *in vivo*, the biogenesis of fluorescent conductive protein microfibers via metabolic pathways. By challenging the simple freshwater polyp *Hydra vulgaris* with DTTO, we demonstrate the stable incorporation of the dye into supramolecular protein-dye co-assembled microfibers without signs of toxicity. An integrated multilevel analysis including morphological, optical, spectroscopical, and electrical characterization shows electrical conductivity of biofibers, opening the door to new opportunities for augmenting electronic functionalities within living tissue, which may be exploited for the regulation of cell and animal physiology, or in pathological contexts to enhance bioelectrical signaling.**

## INTRODUCTION

Protein-based nano/microfibers are currently matter of great interest as advanced biomaterials for a variety of applications, from tissue regeneration to drug delivery and bioelectronics. Several studies have been reported describing the *de novo* engineering and *in vitro* preparation of these systems (Frezzo and Montclare, 2015; Hume et al., 2014; Kamada et al., 2017; McNamara et al., 2017; Xu et al., 2015). Studying the properties of protein-based nano-/microfibers and the mechanisms of formation of their hierarchical supramolecular structures is expected, on one side, to extend our capability to design high-performance biomaterials and, on the other, to improve our knowledge on the formation of protein aggregates related to neurodegenerative pathologies such as Parkinson, Alzheimer, and prion diseases. Recently, microfibers of collagen and elastin have been prepared by self-assembly of precursor nanofibrils using a microfluidic set up, the assembly mechanism elucidated, and the microfibers used as building blocks for the fabrication of biomaterials for tissue engineering (Kamada et al., 2017). A few *de novo* proteins capable to self-assemble into nano-/microfibers have been prepared and their secondary structure analyzed by a variety of techniques; the engineered protein coiled-coil secondary structure was found to be capable to incorporate hydrophobic small molecules such as curcumin, a cancer therapeutic agent (Hume et al., 2014), and the protein microfibers were checked for drug delivery (Frezzo and Montclare, 2015). Micron-sized silk fibers embedded into a chitosan membrane showed improved repair efficiency for wound healing *in vivo* (Xu et al., 2015). Nevertheless, although it is proved that it is possible to prepare *in vitro* proteins with programmed structural motifs, capable to self-assemble into desired supramolecular structures, it is still a major challenge to achieve the same level of structural variety, precision, and specificity as native proteins in living organisms. One way to attain the objective would be to find the means to induce living organisms to physiologically form *in situ* biomolecules with new properties via recognition and incorporation of specific nontoxic small molecules introduced from outside. Recently, the complex internal structure of plants has been used as a template for *in situ* fabrication of electronic circuits by means of conducting polymers and hybrid oligothiophenes inspiring novel bioengineering concepts (Stavrinidou et al., 2015, 2017). Naturally derived proteins are an exceptional alternative to synthetic materials, as they offer favourable sustainability and biocompatibility, in the form of fibers, films, and scaffolds. However, proteins properties and

<sup>1</sup>Istituto di Scienze Applicate e Sistemi Intelligenti "E.Caianello", Consiglio Nazionale delle Ricerche, Via Campi Flegrei, 34, 80078 Pozzuoli, Italy

<sup>2</sup>Istituto per la Sintesi Organica e Fotoreattività, Consiglio Nazionale delle Ricerche, Via Piero Gobetti, 101, 40129 Bologna, Italy

<sup>3</sup>Istituto di Nanotecnologia, Consiglio Nazionale delle Ricerche, c/o Campus Ecotekne – Università del Salento, via Monteroni, 73100 Lecce, Italy

<sup>4</sup>Istituto per la Microelettronica e Microsistemi, Consiglio Nazionale delle Ricerche, Via Pietro Castellino 111, 80131 Napoli, Italy

<sup>5</sup>ESRF, the European Synchrotron, 71 Avenue des Martyrs, Grenoble, France

<sup>6</sup>Present address: Instituto de Ciencia de Materiales de Aragón and CIBER-BBN, Campus Rio Ebro, C/Mariano Esquillor s/n, 50018 Zaragoza, Spain

<sup>7</sup>Present address: Istituto di Scienze Applicate e Sistemi Intelligenti "E.Caianello", Consiglio Nazionale delle Ricerche, Via Campi Flegrei, 34, 80078 Pozzuoli, Italy

<sup>8</sup>Lead Contact

\*Correspondence: [claudia.tortiglione@cnr.it](mailto:claudia.tortiglione@cnr.it)  
<https://doi.org/10.1016/j.isci.2020.101022>



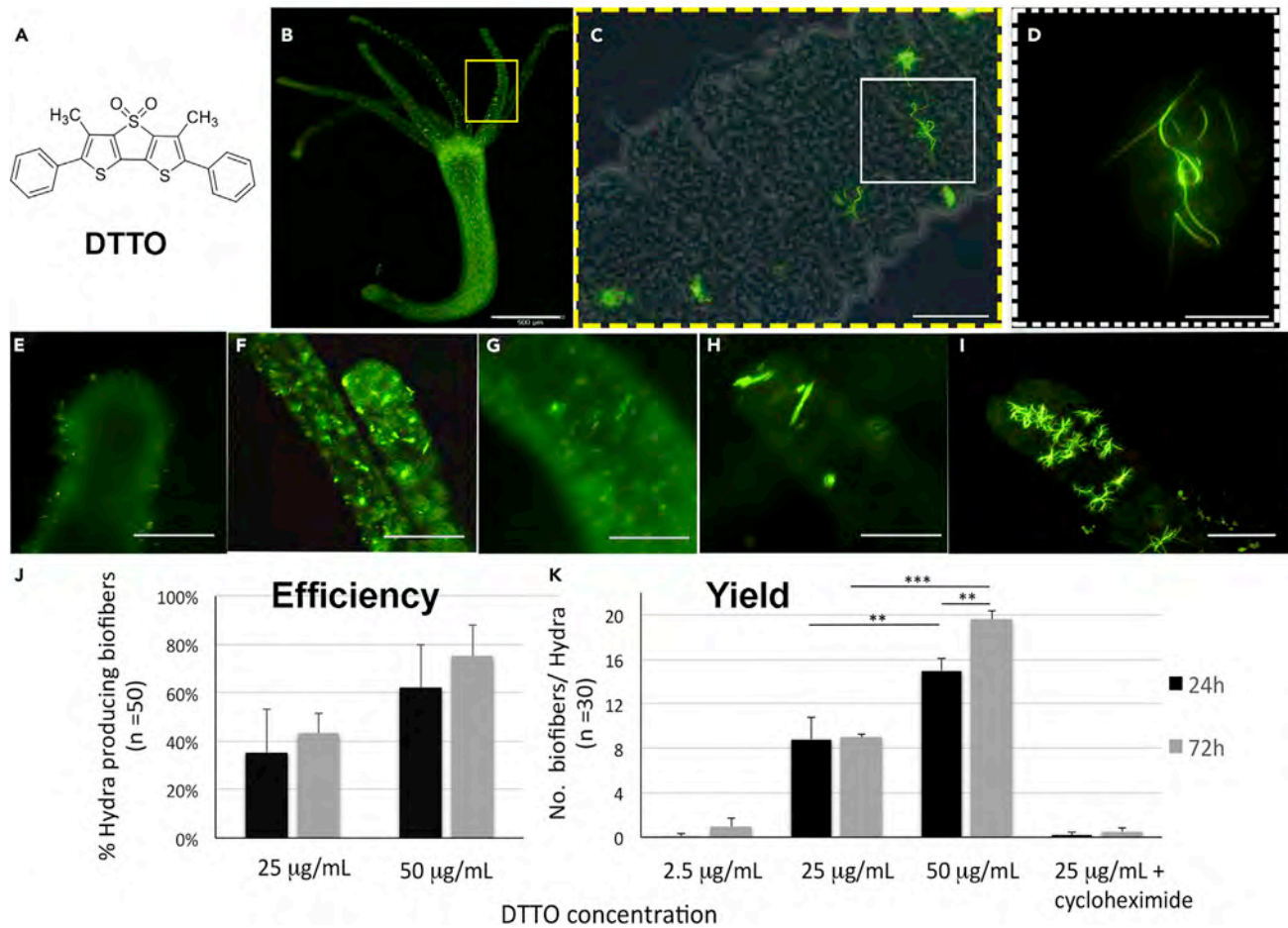


**Figure 1. In Vivo Production of Fluorescent Biofibers from DTTO**

(A) Molecular structure of the green fluorescent semiconducting dye DTTO.

(B–D) (B) *In vivo* fluorescence image of a polyp incubated with DTTO in *Hydra* medium for 24 h. Both a diffuse- and a granular-patterned fluorescence label the whole animal. The tentacle region within the yellow rectangle is shown at higher magnification in (C) optical and fluorescence-merged image of the tentacle showing highly fluorescent green fibers. See also Figure S6 and Videos S1 and S2. An example of a single biofiber (as that inside the white rectangle) is shown at high magnification in (D) a fluorescent biofiber presenting linear, bent, and coiled regions. (E–H) Dynamics of biofiber production. Animals were pulsed 5 h with DTTO (25 µg/mL) and continuously monitored.

(E–I) (E) At time zero p.t. only granular spots are detectable, whereas after (F) 24 h linear fibers are produced inside the tentacles, of length progressively increasing after (G) 3 days and (H) 6 days p.t. (I) DTTO concentration equal to 50 µg/mL increases the average number of biofiber detected into the tentacles. Scale bars, 500 µm in B; 20 µm in C and D; 100 µm in E–I.

(J) Efficiency of biofiber production in relation to DTTO concentration and incubation time. Data represent the average ±SD of three independent experiments (n = 50). Statistical evaluation performed using Student t-test indicates no significance.

(K) DTTO-treated polyps were fixed and mounted on microscopy slides for biofiber detection. Data represent the average ±SD of three independent experiments (n = 30). Statistical comparisons were performed using unpaired t test; \*p < 0.05; \*\*p < 0.01; \*\*\*p < 0.001. p values are reported for all conditions in Table S1.

functions are strictly related to the characteristics of their hierarchical supramolecular structure, so the introduction of exogenous elements in living organisms should not perturb the assembly mechanism. In recent years, we have reported that treating different lines of living cells (NIH 3T3, HeLa, B104) with a dilute solution of the fluorescent semiconducting dye 3,5-dimethyl-2,3'-bis(phenyl)dithieno[3,2-b;2',3'-d]thiophene-4,4-dioxide (DTTO, Figure 1A), capable to spontaneously cross the cell membrane and be recognized by specific intracellular proteins, the physiological formation of fluorescent conductive protein microfibers takes place without causing any significant effect on cell viability and proliferation (Palama et al., 2011; Viola et al., 2013). The physiologically produced protein microfibers, used as biomaterials to seed living cells, induced different fate in terms of cellular morphology, viability, and cytoskeleton rearrangement (Palama et al., 2015). We report here a further and more important step in our search for the

production of functional microfibers *in vivo*, in a noninvasive way, namely the production of protein-DTTO co-assembled fluorescent conducting microfibers in the small freshwater model *Hydra vulgaris*. At the base of metazoan evolution the polyp *Hydra vulgaris* is a very simple animal, shaped as a hollow tube whose walls are made by a two-cell thick layer, i.e. an outer epithelial cell sheet, the ectoderm, and an inner epithelial cell sheet, the endoderm (Galliot and Schmid, 2002). Stem cells interspersed between these two layers ensure continuous cell turnover and differentiation of only a few types of specialized cells (neurons, gland cells, nematocytes) (Hobmayer et al., 2012). The tissue plasticity and the capability to regenerate amputated body parts made this organism a well-established model for developmental and stem cell biology (Holstein et al., 2003). Recently, the tissue-like organization, the absence of organs, and biological fluids posed the bases to use *Hydra* to test toxicity and bioactivity of a variety of nanomaterials and nanodevices (Allocca et al., 2019; Ambrosone et al., 2016; Moros et al., 2018; Tortiglione et al., 2017). With the aim to translate the *in vivo* capability of DTTO monomers to self-organize into supramolecular structures, which could functionally affect/modulate the overall physiology, here we soaked *Hydra* polyps in their culture solution containing DTTO and found in a few days the spontaneous production of microfibers that were in part secreted into the medium. A detailed physico-chemical characterization of these fibers demonstrated their protein-based structure and, more importantly, their conductive behavior, which could be exploited as a novel biocompatible source of endogenously produced materials for bioelectronics. Overall we propose a simple and effective strategy to manipulate physiological processes *in situ*, by spontaneous engineering of endogenous components, leading to a new class of hybrid-protein-based materials with electrical functionality. The introduction of a new electronic functionality into a living animal may represent an unprecedented tool to regulate physiological function, from cell signaling to tissue regeneration and neuronal transmission and a valid alternative to genetic manipulation. Tissues with integrated biocompatible electronics, manufactured *in vivo* in localized regions, may inspire new devices to manipulate biological functions by adding or augmenting conductivity in physiological or pathological contexts with spatiotemporal control, paving the way to new bioengineering concepts.

## RESULTS

### **In Vivo Biosynthesis of Biofibers from Green Fluorescent Semiconducting Thiophene Dye DTTO**

Preliminary analyses were performed to test potential toxic effects played by DTTO on living *Hydra*. The dose range was initially selected on the bases of our previous results obtained in cell cultures (Palama et al., 2011, 2015), where a 25  $\mu\text{g}/\text{mL}$  dose supplied for 5 h was found biocompatible and effective for fiber formation. Dose response evaluations were performed under chronic or acute conditions, up to 72 h. Figure S1 shows dose-response curves and *in vivo* fluorescence imaging obtained in chronic condition, i.e. by continuously treating animals with DTTO or with ECB04, another thiophene-based compound previously shown unable to induce fiber formation in cells (Palama et al., 2011). Both compounds showed similar toxicological profile, i.e. the appearance of behavioral and morphological alterations from 24 h of continuous incubation onwards, while higher doses were lethal at this time point. Next we analyzed the effect induced by increasing doses of DTTO (2.5, 25, and 50  $\mu\text{g}/\text{mL}$ ) exposed for a limited period (5 h, acute condition) to *Hydra* by using several *in vivo* and *in vitro* approaches (Figures S2 and S3) and detected slight effects only at the highest dose, when the morphology was transiently affected. The 25  $\mu\text{g}/\text{mL}$  dose was confirmed fully biosafe, as previously observed in cells, and was used for following analyses. At this dose, a spotted granular-like fluorescence was detected inside animal tissues (Figure 1B), probably due to dye accumulation into storage vacuoles, as observed for other microbeads and inorganics nanoparticles (Marchesano et al., 2013; Tortiglione et al., 2009). A similar pattern was observed in presence of ECB04 and two other fluorophores (Figures S1, S4, and S5) presenting similar thiophene-based backbone but different lateral moieties replacing the phenyl group in position X (Scheme S1). These fluorophores, shown to induce fluorescent fiber formation in NIH3T3 cells (Palama et al., 2011), accumulated into *Hydra* tissues producing intense and diffuse staining. Remarkably, only in the tentacles of animals treated with DTTO long and highly fluorescent fibers (from here biofibers, i.e. produced in *Hydra*), mostly aligned perpendicular to the tentacle axis, were found. The biofibers detected on the external surface of the tentacle cells and embedded between the cells showed diverse shapes, length, and structures—either linear, branched or hooked (Figures 1C, 1D, and S6, Videos S1 and S2). Spontaneous aggregation of DTTO in *Hydra* medium was indicated by the presence of round–short fibril-shaped fluorescent aggregates (Figure S7), remarkably different from those detected in *Hydra* tissue and never presenting coiled structures. In order to study the dynamics of biofiber formation the animals were pulsed for 5 h with DTTO, extensively washed to remove any dye from the medium, and then continuously inspected. At the beginning of the monitoring, a diffuse

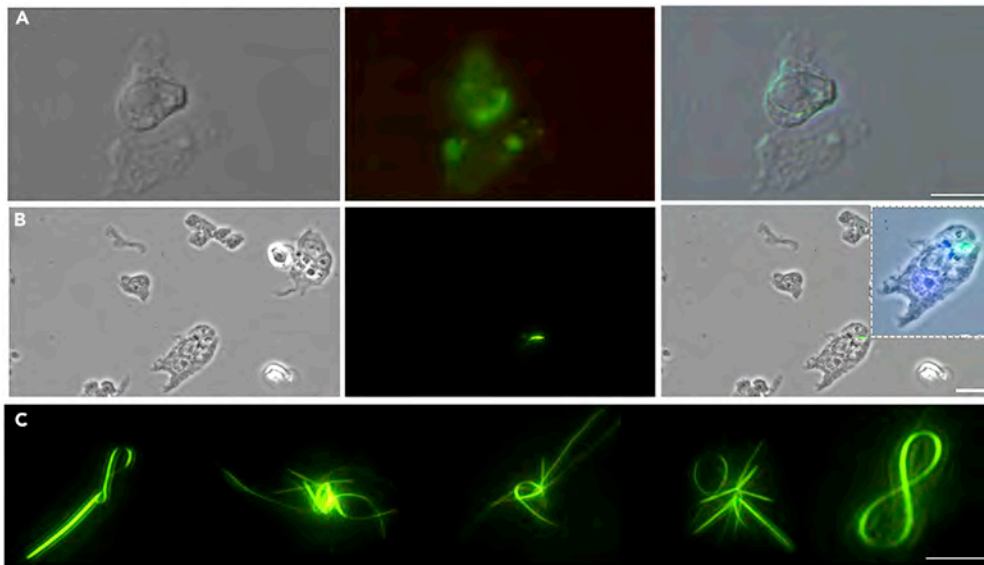


**Figure 2. Characterization of Fluorescent Biofibers from Macerated Hydra**

Animals 72 h p.t. were dissociated into a suspension of single cells, fixed and imaged using phase contrast (left column) and fluorescence microscopy (central column). Right column displays the overlay of both images.

(A and B) (A) Picture of a nematocyte containing a green emitting fiber and (B) a group of cells, showing a fiber inside an ectodermal epithelial cell. Nuclei counterstained with DAPI appear in blue in the inset. Scale bars, 10  $\mu\text{m}$  in A, 20  $\mu\text{m}$  in B.

(C) Fluorescence microscopy of fibers present into the macerated solution. Several structures are formed, presenting both linear and bent motifs, of average length higher than biofibers.

See also [Figure S7](#).

fluorescence was detected in the external layer of the *Hydra* together with green granular spots ([Figure 1E](#)), progressively increasing with the incubation time and detectable inside ectodermal cells. At 24 h post-treatment (p.t.), in addition to this punctuated pattern, microfibers of about 20  $\mu\text{m}$  length were found in the tentacles ([Figure 1F](#)) and could be observed up to 6 days p.t. ([Figures 1G and 1H](#)), whose length increased with time. In the rest of the body only the punctuated fluorescence but not the fibers was detectable. The formation of long microfibers observed with DTTO and not with other thiophene-based compounds, such as ECB04 and compounds 2–3, with backbones similar to those of DTTO, suggests specific bioactivity of the latter in promoting endogenous fiber production. Clearly, the presence of two lateral phenyl groups in the molecular structure appears to be a necessary requirement to promote dye-protein co-assembly.

The efficiency of the biofiber production ranged from 35% (lowest dose, 24 h p.t.) up to 75% (highest dose, 72 h p.t.), indicating a variability among individuals and suggesting at the same time that the supramolecular dye-protein co-assembly could rely on an active mechanism ([Figure 1J](#)). The yield of this process (number of biofibers/*Hydra*) was shown as concentration and time dependent, ranging from less than 1 biofiber/*Hydra* produced by lowest DTTO dose (2.5  $\mu\text{g}/\text{mL}$ ) up to  $19 \pm 0.7$  biofibers produced at 72 h in the presence of 50  $\mu\text{g}/\text{mL}$  ([Figure 1K](#) and [Table S1](#) for evaluation of statistical significance between all conditions). Relative images are shown in [Figure S8](#). These data prompted us to investigate whether or not the mechanism of biofiber production involved any active metabolic pathway, such as the protein synthesis. *Hydra* polyps were pre-treated 2 h with cycloheximide, a known inhibitor of the protein synthesis ([Obrig et al., 1971](#)), before DTTO addition. The graph of [Figure 1K](#) shows a strong inhibition of the biofibers production, as only a few biofibers could be detected in treated polyps, suggesting the protein-based structure of the DTTO biofibers ([Figure S9](#)). [Figure 2](#) displays the fluorescence microscopy images of cell suspensions obtained by maceration of treated animals. This procedure allows dissociating the animal in single cells, preserving their morphology for microscopic analysis. Short fluorescent fibers were detected inside nematocytes ([Figure 2A](#)), the stinging cells located in the tentacles, and body ectodermal cells ([Figure 2B](#)) indicating the capability of diverse cell types to initiate the assembling of these structures. Maceration of animals treated with compounds 2 and 3 did not reveal the presence of any biofiber but only fluorophore

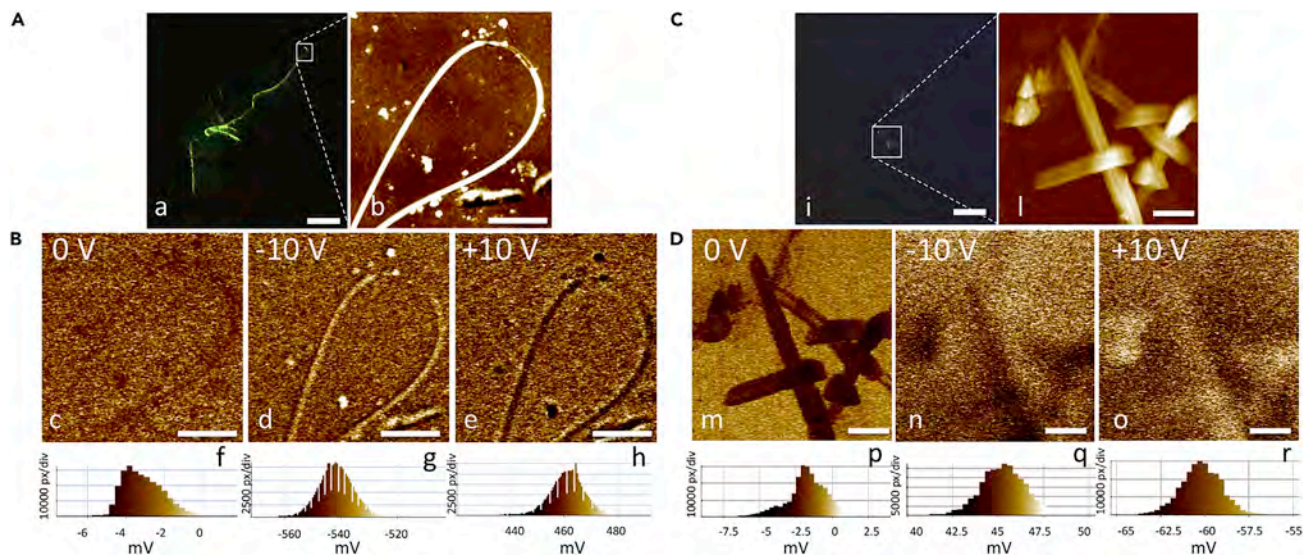


**Figure 3. Morphological and Electrical Characterization of Biofibers**

(A) Fluorescence image of (a) a biofiber deposited on a conductive substrate (scale bar, 20  $\mu\text{m}$ ). The white square shows the sub-region selected for AFM and EFM characterizations. (b) AFM topography showing a typical loop structure found in the biofibers (scale bar, 2  $\mu\text{m}$ ).

(B) EFM amplitude of the biofiber at bias voltage (c) 0 V, (d)  $-10$  V, and (e)  $+10$  V, respectively (scale bar, 2  $\mu\text{m}$ ). The morphology of the sample appears when a bias voltage is applied. EFM amplitude distribution at bias voltage: (f) 0 V, (g)  $-10$  V, and (h)  $+10$  V, respectively. The Gaussian distribution shows that the average level is proportional to the applied voltage, indicating the conducting or semiconducting nature of the sample.

(C) Fluorescence image (i) of a control fibril fragment, formed by aggregation of DTTO alone in Hydra medium, deposited on a conductive substrate (scale bar, 10  $\mu\text{m}$ ). The white square shows the sub-region selected for AFM and EFM characterizations. (l) AFM topography (scale bar, 1  $\mu\text{m}$ ).

(D) EFM amplitude of the control at bias voltage (m) 0 V, (n)  $-10$  V, and (o)  $+10$  V, respectively (scale bars, 1  $\mu\text{m}$ ). The morphology of the sample is clearer when bias voltage does not apply. EFM amplitude distribution at bias voltage: (p) 0 V, (q)  $-10$  V, and (r)  $+10$  V, respectively. The average level is quite the same for all applied voltage, indicating the insulating nature of the sample.

See also [Figure S10](#).

accumulation into vesicle-like structures, representing stable structures devoted to garbage storage, before external secretion ([Figure S5](#)). Long and highly structured biofibers were by contrast observed upon treatment with DTTO into the macerated solution but never included into the cells, suggesting either their degradation into small pieces due to the mechanical forces used for tissue maceration or that their growth and sterical structuring occurs during the secretion pathway. In [Figure 2C](#) laser scanning confocal microscopy images of several biofibers are reported, showing straight and bent motifs alternating and interlaced into the same biofiber, displaying large aspect ratios and an average length of 59  $\mu\text{m}$ , in contrast with the structures formed by DTTO self-assembled in Hydra medium (13  $\mu\text{m}$ ), as determined in the graph of [Figure S7](#). The two microstructures also showed a different photobehavior, biofibers being more stable (maintained their shape and high fluorescence up to two years from biosynthesis) and resistant to UV illumination, compared with structures spontaneously formed by DTTO in Hydra medium ([Figure S7](#)). Beside morphological characterization by fluorescence microscopy, optical and electrical properties of biofibers were characterized by a variety of techniques, including atomic force microscopy (AFM), electrostatic force microscopy (EFM), synchrotron fourier transform infrared micro-spectroscopy (IMS), X-ray photoelectron spectroscopy (XPS), UV-Vis, photoluminescence (PL), and circular dichroism (CD). Cells and floating fibers obtained by maceration of treated animals (5 h DTTO treatment and 72 h p.t.), concentrated by centrifugation, were used for all approaches and compared with macerates from untreated *Hydra* (control) and with supramolecular structures formed spontaneously by DTTO in animal-free medium.

### Atomic and Electrostatic Force Microscopy Characterization

EFM measures local Coulomb electrostatic interaction between the conductive tip and the sample, when a bias voltage is applied on the tip. Such a local interaction can be detected as oscillation amplitude and phase of the EFM probe ([Rea et al., 2016](#); [Kader et al., 2005](#)). Green fluorescent fibers obtained from macerates were first localized by fluorescence microscopy and then the region of interest examined by AFM ([Figure 3A](#), section a, b) and EFM ([Figure 3B](#)). AFM topographies on a  $1 \times 1 \mu\text{m}^2$  field are shown in [Figure S10](#), where the morphology, a line profile, and pointed properties are presented for both a biofiber

and a DTTO aggregate. For the biofiber the estimated sizes were about 60 nm high and 235 nm wide (Figure S10). The EFM was performed on the same field of AFM, applying a bias voltage 0 V, -10 V, and +10 V. The amplitude EFM image without voltage application identifies shadowed features mirroring sample morphology (Figure 3B, section c, Figure S10), whereas, when bias voltage of -10 V and +10 V is applied a clear contrasted morphology becomes evident, with bright and dark zones mirroring the fiber morphology (Figure 3B, section d and e, respectively). The EFM amplitudes showed Gaussian distributions (Figure 3B, sections f-h) centered on an average level, which is directly proportional to the applied bias voltage. These features indicate the current flow correlated to a conducting or semiconducting behavior of the sample. For comparison, also the structures formed by aggregation of DTTO alone in *Hydra* medium at the same concentration over the same incubation time were examined. The results are reported in Figures 3C, 3D, and S10. These fibers show completely different features and electrical behavior. DTTO tends to self-assembly in round fibril-shaped aggregates. Figure 3C, image i, shows a very short fluorescent fibril and the region where the AFM and EFM characterizations were performed. AFM topography (Figure 3C, section l) shows shorter but wider fibrils about 3–5  $\mu\text{m}$  long, 130 nm high, and 420 nm wide (see also Figure S10). Also in this case, the EFM images have been performed with a bias voltage 0 V, -10 V, and +10 V, respectively (Figure 3D, sections m, n, o, and Figure S10). In the amplitude EFM (Figure 3D, section m) the morphology of the control sample is clearly identified at 0 V bias voltage, whereas, when bias voltage of -10 V and +10 V is applied, the morphology becomes less clear and shows a kind of inverse polarization (Figure 3D, sections n, o), probably due to the opposite polarization of dipole distribution in an insulating behavior. Moreover, the EFM amplitude distributions for -10 V and +10 V are centered on average levels that are only slightly different from the average level at 0 V (Figure 3D, sections p, q, and r), indicating that the flowing current is similar for all applied voltages. Altogether this evidence shows a DTTO unique behavior featuring the biofibers, clearly distinguishable by the self-assembled DTTO, indicating a specific property added to the fiber by the cell machinery, *in vivo*.

#### Fourier Transform Infrared Micro-spectroscopy

A macerated solution from DTTO-treated animals, containing fixed cells and floating biofibers, was analyzed by IMS using synchrotron light as source (Ling et al., 2011). The infrared spectrum of protein contains two characteristic absorption bands of particular pertinence to protein secondary structure, the absorptions associated to C=O stretching denoted as amide I ( $\approx 1655\text{--}1620\text{ cm}^{-1}$ ) and those associated to N-H bending denoted as amide II ( $1547\text{ cm}^{-1}$ ). The C=O and N-H functional groups involved in hydrogen bonding between protein moieties influence the positions of both amide I and amide II, hence these bands are sensitive to secondary structure composition. In particular, the position of amide I is a very useful predictor of protein secondary structure with band assignment regions for  $\alpha$ -helix structure ( $1648\text{--}1657\text{ cm}^{-1}$ ) and  $\beta$ -sheet ( $1623\text{--}1641\text{ cm}^{-1}$ ) (Miller et al., 2013). The IMS results showed the protein-based nature of a biofiber, giving the characteristic amide I and amide II absorption bands. From Figure 4A it can be observed that the amide I absorbance ( $1655\text{ cm}^{-1}$ ) corresponds to the location of the biofibers. In Figure 4C the comparison of extracted IR spectra from fiber and outside the fiber provides more details about the protein structure composed of mixed  $\alpha$ -helix and  $\beta$ -sheet as evidenced by the intense absorptions in the fiber spectrum at  $1655\text{ cm}^{-1}$  and  $1624\text{ cm}^{-1}$ . IMS has been successfully used for investigations in cells and tissue where the same absorption bands from amides identified in this study (in particular amide I) have been used to determine protein misfolding and aggregation of amyloid plaques, infectious prion proteins,  $\alpha$ -synuclein, and tau proteins (Miller et al., 2013).

#### X-Ray Photoelectron Spectroscopy

In order to have evidence of the supramolecular incorporation of DTTO inside proteins XPS measurements were performed on pure DTTO and biofibers from *Hydra* macerates. The results are reported in Figure 4 and Table S2. The S 2p peak is a fingerprint for DTTO on Au substrates and the presence of two doublets of S  $2p_{3/2}$ , i.e. S=O group at 168.5 eV and S-C group at 164.8 eV, is in excellent agreement with the spectra reported in previous work on oxidized thiophene-based materials (Figure 4E) (Di Maria et al., 2017). Moreover, the stoichiometric ratio between Sulphur-Carbon (S-C)- and Sulphur-Oxygen (S=O)-bonded species was close to the expected value of 2 ( $1.8 \pm 0.2$ ). The XPS spectrum of the biofibers from *Hydra* macerates deposited on a gold substrate confirmed the presence of the S  $2p_{3/2}$  peak, with the S=O component at 168.5 eV and the S-C component slightly reduced at 163.8 eV probably due to fiber formation. Additionally, the chemical shift of N 1s at 400.5 eV, related to the protein material contained in the fiber, was observed together with that of P  $2p_{3/2}$  at 134.2 eV, compatible with phosphate groups (P=O) associated to the phospholipid bilayer (Figures 4D and 4F) (Wagner et al., 1997). The presence of significant amounts of protein

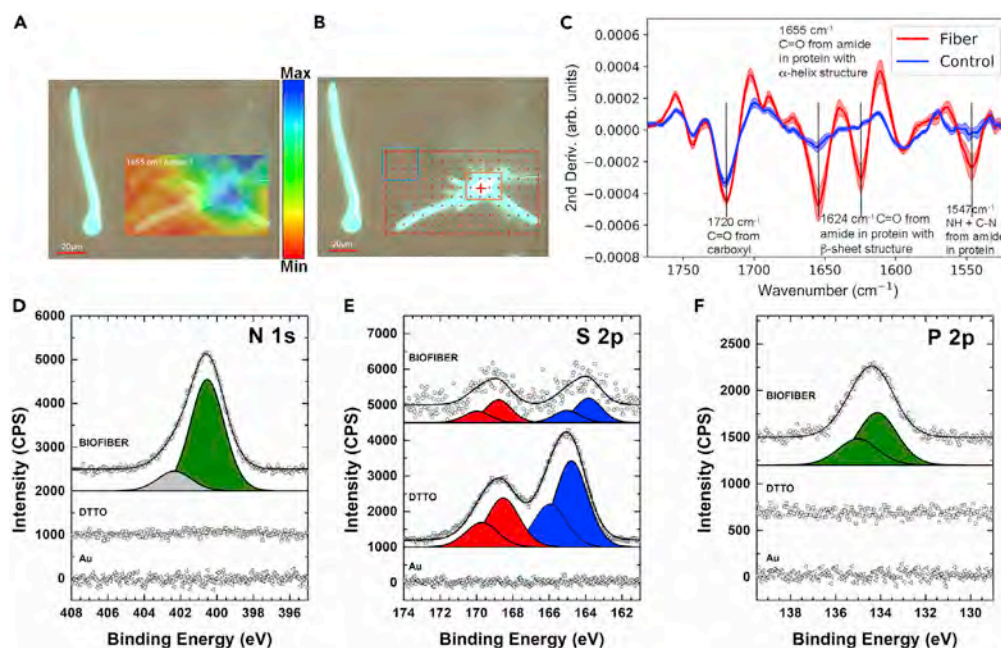


**Figure 4. Synchrotron Infrared Microspectroscopy and X-ray Photoelectron Spectroscopy of a Single Green Fluorescent Biofiber**

(A) Image of a UV illuminated biofiber and IMS image at  $1655\text{cm}^{-1}$  showing the distribution of amide I bond from protein. For interpretation of the amide I bond signal intensity, a pseudocolor scale bar is introduced, where blue represents the highest intensity and red the lowest. Scale bar,  $20\ \mu\text{m}$ .

(B) The red box is the mesh used for IR mapping, the blue box is the control region, and the orange box is the biofiber region where IR spectra were extracted. Scale bar,  $20\ \mu\text{m}$ .

(C) Averaged second derivative IR spectra of the control and fiber regions.

(D–F) (D) N 1s, (E) S 2p, and (F) P 2p XPS spectra of  $\text{Ar}^+$  sputtered Au (triangles), DTTO on Au (squares), and biofibers (circles). S 2p presents two doublets associated to S=O bond (red) and S-C bond (blue). In all peaks the background was subtracted and a constant value added to order the samples. S 2p and P 2p were fitted by doublets in fixed energy shift ( $2p_{3/2}$  and  $2p_{1/2}$ ). Signal of S 2p of biofibers was multiplied by a factor 10. See also Table S2.

and phospholipid materials justifies the low S 2p signal from biofibers (0.25%, Table S2). This suggests that inside biofibers DTTO is surrounded by a layer of protein and phospholipid materials with a thickness in the same order of magnitude of the XPS probe depth (up to 10 nm).

### Optical Characterization

The photophysical characterization of the biofibers produced by living animals was obtained by UV-vis, photoluminescence (PL), and circular dichroism spectroscopy (CD) and compared with those produced by DTTO self-aggregated in organic solvent and Hydra medium. Table 1 shows that  $\lambda_{\text{exc}}$ ,  $\lambda_{\text{PL}}$  and the lifetimes  $\tau_1$  and  $\tau_2$  of DTTO self-assembled in Hydra medium are deeply different from those measured in macerates containing isolated biofibers. Particularly significant is the value of the fluorescence anisotropy, which passes from 0 for the former to 0.25 for the latter. The large value of fluorescence anisotropy in sample A (biofiber) suggests that DTTO is embedded into a highly anisotropic supramolecular structure. Figure 5 reports the excitation, PL, and CD spectra of macerates containing isolated biofibers (black plot) and the macerates of untreated Hydra used as a control (red plot). The absorption spectra of the samples are characterized by a large amount of scattering hiding the absorption signals (Figure S10). Thus, the excitation spectra—displaying the frequencies generating the photoluminescence spectrum and corresponding to the frequencies absorbed by the system—were measured applying a fixed excitation wavelength of 500 nm (Figure 5A). The comparison of DTTO parameters relative to the biofibers with those of DTTO in methylene chloride (Figure S10) shows unambiguously the signature of the dye in the fibers. In particular, the photoluminescence spectra of the samples indicate a Stokes shift between absorption and emission spectra amounting up to 100 nm, a value in line with what has already been observed for DTTO in organic solution (Palama et al., 2011).

Sample	$\lambda_{\text{abs}}$ (nm)	$\lambda_{\text{exc}}$ (nm) <sup>a</sup>	$\lambda_{\text{PL}}$ (nm) <sup>b</sup>	$\tau_1$ (ns) <sup>c</sup>	$\tau_2$ (ns) <sup>c</sup>	Fluorescence <sup>d</sup> Anisotropy
A <sup>e</sup>	–	395	500	2.2	8.1	0.25
B <sup>f</sup>	408	–	514	16.17	–	~0
C <sup>g</sup>	–	350	425;575	1.2	4.4	~0

**Table 1. Photophysical Characterization of Biofibers Formed in *Hydra* and DTTO Aggregates Formed in Culture Medium**

Characterization was performed on (A) biofibers, (B) DTTO in methylene chloride, and (C) DTTO aggregated in *Hydra* medium.

<sup>a</sup>Excitation spectrum obtained with a fixed emission wavelength of 500 nm.

<sup>b</sup>Maximum of photoluminescence emission ( $\lambda_{\text{exc}} = 395$  nm).

<sup>c</sup>Fluorescence lifetimes.

<sup>d</sup>Steady state fluorescence anisotropy.

<sup>e</sup>Cell suspension and floating biofibers.

<sup>f</sup>DTTO in methylene chloride (molar extinction coefficient  $\epsilon = 18,000 \text{ M}^{-1}\text{cm}^{-1}$ ; fluorescence quantum yield = 0.83).

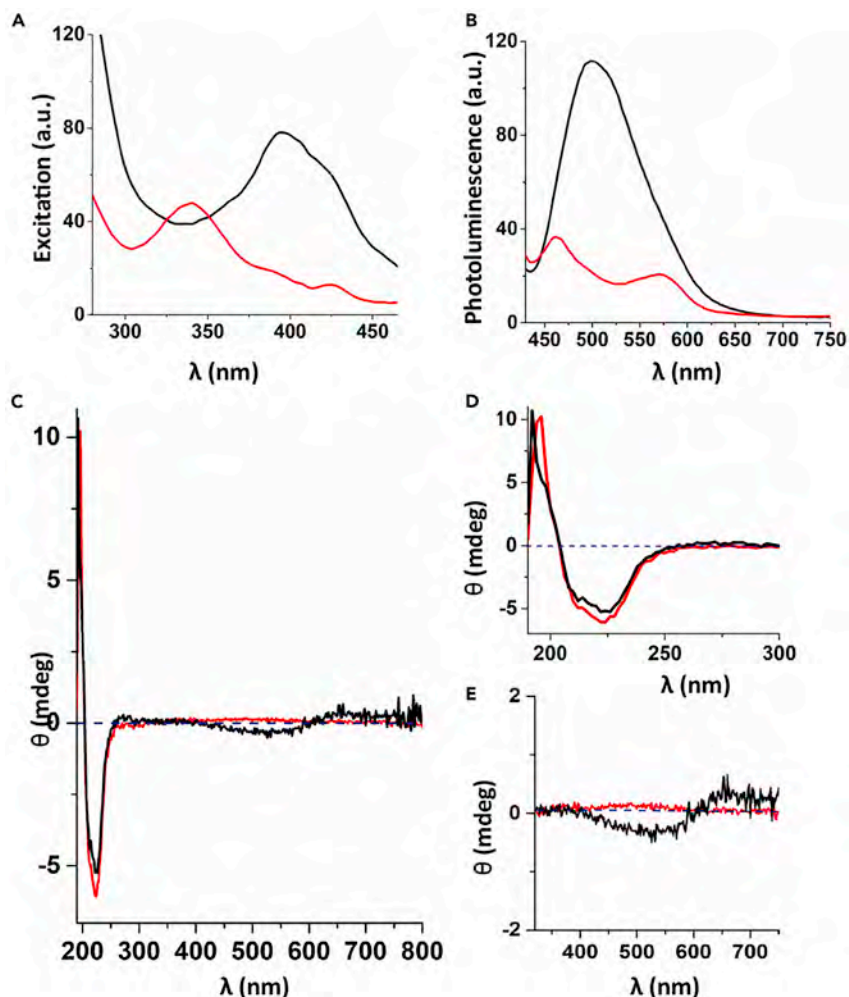
<sup>g</sup>DTTO self-assembled in *Hydra* medium (CaCl<sub>2</sub> 1mM, 0.1mM NaHCO<sub>3</sub>).

Figure 5C shows the CD spectrum of the macerates containing biofibers presenting a signal with negative Cotton effect in the region 190–240 nm and a less intense signal in the region 400–600 nm, indicating chiral content in both regions of the sample. On the contrary, the control sample (untreated *Hydra*) displayed only one signal with negative Cotton effect in the region 200–220 nm superimposable to that of the treated *Hydra*. The CD signal in the 190–240 nm region (see magnification Figure 5D) is mainly due to protein peptide bond with an  $n \rightarrow \pi^*$  transition centered around 220 nm and a  $\pi \rightarrow \pi^*$  transition around 190 nm (Greenfield, 2006; Holzwarth and Doty, 1965; Kelly et al., 2005). The less intense signal observed in DTTO treated *Hydra* in the region 400–600 nm (see magnification Figure 5E) corresponds to the absorption region of DTTO. CD spectroscopy is extensively used to study the secondary structure of proteins in solution, which is very sensitive to the environment, temperature, or binding interactions with other molecules and can furnish structural, kinetic, and thermodynamic information (Kelly et al., 2005; Greenfield, 2006; Holzwarth and Doty, 1965). The CD signal in the region 190–220 nm is characteristic of  $\alpha$ -helix protein secondary structure, whereas the signal in the region 400–600 nm is a strong indication of the presence of DTTO embedded into the supramolecular structure of some proteins. Indeed, it is well known that in addition to the intrinsic CD of the protein backbone, small molecules interacting with the proteins show extrinsic CD bands indicative of such an interaction (Kelly et al., 2005; Greenfield, 2006; Holzwarth and Doty, 1965; Di Maria et al., 2014). Thus, although DTTO is an intrinsically achiral molecule, the proximity of the proteins causes the appearance of an induced CD signal pertaining to the fluorophore. Moreover, it cannot be excluded that such a signal also reflects the chiral supramolecular organization of the dye driven by the proteins themselves.

In an attempt to identify the protein composition of the biofiber we used *Hydra* anti-collagen-specific antibody in immunolocalization experiments on macerates from DTTO-treated *Hydra*. Results failed to detect any cross-reactivity (Figure S6C), opening the possibility that other proteins may be bound to the DTTO monomer structuring the fluorescent biofiber. We cannot rule out the possibility that the epitope can be masked due to DTTO bonding or due to the tissue maceration process.

## DISCUSSION

Our data unambiguously indicate that DTTO is biocompatible and inside *Hydra* tissue spontaneously co-assembles with proteins giving rise to the formation of fluorescent and conductive microfibers. Interestingly, the biofiber formation is specific for DTTO, as other oligothiophene derivatives were not able to produce them. We have already observed the spontaneous co-assembly of DTTO with proteins inside specific cell lines such as living fibroblasts of different origin, where DTTO is incorporated within type-I collagen's triple helix (Palama et al., 2011), and mouse neuroblastoma cells (B104), where the fluorophore is incorporated within vimentin's supramolecular structure (Palama et al., 2015). Most probably, in the present case bundles of microfibers are spontaneously formed where DTTO is incorporated within different types of cells. This hypothesis is supported by the *Hydra* anatomy, composed of three stem cell lineages, i.e. ectoderm, endoderm, and interstitial stem cell lineage, including self-renewing cells and differentiating



**Figure 5. Optical Characterization of DTTO-Based Biofibers**

(A) Excitation spectra obtained by irradiating at 500 nm.

(B and C) (B) Photoluminescence spectra and (C) CD spectra relative to a cell suspension of biofibers (black line) and macerates of untreated *Hydra* (red line).

(D and E) (D) Enlargements of CD spectra (C) in the 180–300 nm and (E) in the 350–750 nm regions.

See also [Figure S10](#).

products, such as gland cells, gametes, nematocytes, and neurons. After maceration of DTTO-treated animals the fluorescent microfibers could be detected in epitheliomuscular cells and nematocytes, suggesting that they might be formed by a variety of proteins coming from different cellular types rather than from a single cell type, and this hampers the identification of a unique protein into the fiber. This raises questions about the mechanism of formation of the microfibers, in particular about (1) the recognition process of the dye by the different proteins and (2) about the molecular and supramolecular processes taking place separately or simultaneously as in the case of spider silk and live cells ([Rising and Johansson, 2015](#); [Palama et al., 2011](#)). As to the first point, a primary role is certainly played by the  $\text{SO}_2$  group of the fluorophore with two oxygens capable of multiple interactions with neighboring hydrogens, as suggested by previous calculations on a model simulating a collagen strand ([Palama et al., 2011](#)). As to the second point, the biofibers showing higher complexity and size were detected in *Hydra* macerates either as floating fibers, or bound to the external part of tissue fragments deriving from tentacles, suggesting that the growth and supramolecular structuring may take place specifically in the tentacles and during the secretion process. However, further investigations are required before a satisfying interpretation can be given on both points. Inside cells only short fluorescent fibers were found inside cells; however, we could not rule out that mechanic forces employed for animal dissociation affect stability of supramolecular folding and cause fiber

fragmentation. Due to the lack of protocols to immortalize and culturing *Hydra* cells *in vitro*, the maceration of whole animal represents, up to date, a valuable and broadly used method to analyze single cells and structures released from the tissue bilayer architecture. Following this approach, we performed accurate characterization of fibrils, both inside cells and on the external side of cells or tentacles, yet preserving their spectacular fluorescence. The conductive behavior of biofibers makes this spontaneous process very fascinating and suggests our model as a new living bioreactor for the production of electroactive materials.

It would be difficult to assign a precise organization at the nanoscale to the proteins' supramolecular structure embedding DTTO. Coexistence of  $\alpha$ -helix and  $\beta$ -sheet secondary structures is common in natural fibrillar proteins (Rising and Johansson, 2015), and our IMS data indicate that both secondary structures are present in the fluorescent biofibers. Although our previous work on live cells indicates that DTTO is embedded within the  $\alpha$ -helix, we do not have any experimental evidence that DTTO can also be embedded into  $\beta$ -sheets. So we cannot say whether the observed fluorescence comes exclusively from  $\alpha$  helices or also from  $\beta$ -sheet configuration.

By using the protein synthesis inhibitor cycloheximide we could prevent biofiber production demonstrating that DTTO drives the formation of hybrid protein-dye microfibers through protein synthesis cell machinery. The microfibers obtained by DTTO self-assembly in *Hydra* medium are morphologically and electrically deeply different from the biofibers. In particular, they are fluorescent but insulating supramolecular structures.

DTTO is a semiconducting conjugated molecule and as most thiophene-based oligomers may display electrical conductivity when organized into appropriate supramolecular structures. Recent evidence reports on hybrid oligothiophenes self-organized in conducting wires along the vascular tissue of a rose plant (Stavrinidou et al., 2017). Here, the supramolecular structure achieved in a living animal by DTTO monomers shows electrical conductivity, as demonstrated by EFM measurements. The incorporation of fluorescence and conductive properties into endogenous building blocks, in part or totally made of proteins, led to the production of novel structures, according to precise dose and time. Under these conditions the DTTO does not interfere with animal viability, suggesting that the fluorophore does not affect biomolecule function.

In conclusion, we show that a simple invertebrate presenting a tissue grade of organization when soaked with a non-toxic fluorescent/semiconducting dye produces fluorescent electroactive protein-dye microfibers having prevalently coiled-coil and a significant contribution of  $\beta$ -sheet secondary structure. By merging multiple techniques, from *in vivo* imaging and single cell analysis, up to optical, spectroscopic, and electrical characterization we demonstrate the possibility to modify endogenous biomolecules into novel hybrid structures showing superior properties. One of the most important applications we foresee for these fluorescent microfibers is their use as biocompatible electroactive scaffolds for bioengineering and tissue regeneration. In particular, biocompatible and biodegradable scaffolds with protein fibers can be used as potentially implantable devices and may contribute to stimulating and controlling neural or muscle activities under electrical stimulation and effectively guide tissue repair. To the best of our knowledge, only a few examples have been reported in which the spontaneous assembly of exogenous organic components has been triggered in whole animals in very complicated environments (Zhao et al., 2018; Zhang et al., 2015; He et al., 2019). The possibility to chemically control, *in vivo*, the formation of micrometer-sized supramolecular architectures provides a new way to bestow additional properties upon the system and has important fundamental as well as applicative implications.

### Limitation of the Study

Model organisms allow prediction studies, testing of chemical compounds, and discovering processes and mechanisms of action but also present innate constraints that limit their use. We demonstrated with *Hydra* the possibility to produce new microstructures modifying *in situ* endogenous proteins, but more functional studies are necessary to evaluate the impact on physiological processes, with or without electrical stimulation, or the induction of new ones. Moreover, both fiber purification and homogeneity need to be implemented. Large-scale purification of the microfibers from the animal tissues is hampered by the tight embedding into membrane/external cuticle, possibly due to chemical composition preventing biofiber release into the medium. Moreover, homogeneity is not possible as biofibers are produced by different

cell types, possibly co-assembling with different proteins. Commercially available antibodies raised against vertebrates and antigens would not easily cross-react with *Hydra* proteins, which justified our use of *Hydra*-specific antibody for immunolocalization. In a future perspective the development of DTTO delivery methods alternative to soaking may drive the homogeneous biofiber production from a specific tissue/cell type.

## METHODS

All methods can be found in the accompanying [Transparent Methods supplemental file](#).

## SUPPLEMENTAL INFORMATION

Supplemental Information can be found online at <https://doi.org/10.1016/j.isci.2020.101022>.

## ACKNOWLEDGMENTS

M.M. acknowledges financial support from the European Union's Horizon 2020 research and Innovation program Marie Skłodowska-Curie grant agreement No. 660228 and the Spanish Juan de la Cierva program. C.T. and H.C. acknowledge European Synchrotron Radiation Facility for access to beam time on the ID21 beam line (experiment MA3261). C.T. acknowledges Prof. Xiaoming Zhang (Baylor College of Medicine, Houston) for the kind gift of *Hydra* anti-collagen type I antibody. F.D.M. acknowledges financial support from the project Molecular Nanotechnologies for Human Health and Environment (PON R&C 611 2007–2013, code PON02\_00563\_3316357) and the EU project INFUSION (Proposal number: 734834).

## AUTHOR CONTRIBUTIONS

C.T., A.T., M.M., and G.B. conceived this project and provided general supervision. M.M., A.T., G.T., and M.B. performed all experiments with *Hydra vulgaris*. F.D.M. and M.Z. performed optical characterization and data analysis, P.D. and L.D.S. performed electrical characterization, H.C.M. and A.K. performed spectroscopic characterization. All authors analyzed and discussed the data and contributed to drafting and editing the manuscript. C.T., M.M., and G.B. finalized the manuscript.

## DECLARATION OF INTERESTS

The authors declare no competing financial interest.

Received: January 23, 2020

Revised: March 17, 2020

Accepted: March 25, 2020

Published: April 24, 2020

## REFERENCES

- Allocca, M., Mattera, L., Bauduin, A., Miedziak, B., Moros, M., De Trizio, L., Tino, A., Reiss, P., Ambrosone, A., and Tortiglione, C. (2019). An integrated multilevel analysis profiling biosafety and toxicity induced by indium- and cadmium-based quantum dots in vivo. *Environ. Sci. Technol.* 53, 3938–3947.
- Ambrosone, A., Marchesano, V., Carregal-Romero, S., Intartaglia, D., Parak, W.J., and Tortiglione, C. (2016). Control of Wnt/beta-catenin signaling pathway in vivo via light responsive capsules. *ACS Nano* 10, 4828–4834.
- Di Maria, F., Fabiano, E., Gentili, D., Biasiucci, M., Salzillo, T., Bergamini, G., Gazzano, M., Zanelli, A., Brillante, A., Cavallini, M., et al. (2014). Polymorphism in crystalline microfibers of achiral octithiophene: the effect on charge transport, supramolecular chirality and optical properties. *Adv. Funct. Mater.* 24, 4943–4951.
- Di Maria, F., Zanelli, A., Liscio, A., Kovtun, A., Salatelli, E., Mazzaro, R., Morandi, V., Bergamini, G., Shaffer, A., and Rozen, S. (2017). Poly(3-hexylthiophene) nanoparticles containing thiophene-S,S-dioxide: tuning of dimensions, optical and redox properties, and charge separation under illumination. *ACS Nano* 11, 1991–1999.
- Frezzo, J.A., and Montclare, J.K. (2015). Exploring the potential of engineered coiled-coil protein microfibers in drug delivery. *Ther. Deliv.* 6, 643–646.
- Galliot, B., and Schmid, V. (2002). Cnidarians as a model system for understanding evolution and regeneration. *Int. J. Dev. Biol.* 46, 39–48.
- Greenfield, N.J. (2006). Using circular dichroism spectra to estimate protein secondary structure. *Nat. Protoc.* 1, 2876–2890.
- He, P.P., Li, X.D., Wang, L., and Wang, H. (2019). Bispirene-based self-assembled nanomaterials: in vivo self-assembly, transformation, and biomedical effects. *Acc. Chem. Res.* 52, 367–378.
- Hobmayr, B., Jenewein, M., Eder, D., Eder, M.K., Glasauer, S., Gufler, S., Hartl, M., and Salvenmoser, W. (2012). Stemness in *Hydra* - a current perspective. *Int. J. Dev. Biol.* 56, 509–517.
- Holstein, T.W., Hobmayr, E., and Technau, U. (2003). Cnidarians: an evolutionarily conserved model system for regeneration? *Dev. Dyn.* 226, 257–267.
- Holzwarth, G., and Doty, P. (1965). The ultraviolet circular dichroism of polypeptides. *J. Am. Chem. Soc.* 87, 218–228.
- Hume, J., Sun, J., Jacquet, R., Renfrew, P.D., Martin, J.A., Bonneau, R., Gilchrist, M.L., and Montclare, J.K. (2014). Engineered coiled-coil protein microfibers. *Biomacromolecules* 15, 3503–3510.
- Kader, M.A., Choi, D., Lee, S.K., and Nah, C. (2005). Morphology of conducting filler-reinforced nitrile rubber composites by

electrostatic force microscopy. *Polym. Test.* **24**, 363–366.

Kamada, A., Mittal, N., Soderberg, L.D., Ingverud, T., Ohm, W., Roth, S.V., Lundell, F., and Lendel, C. (2017). Flow-assisted assembly of nanostructured protein microfibers. *Proc. Natl. Acad. Sci. U S A* **114**, 1232–1237.

Kelly, S.M., Jess, T.J., and Price, N.C. (2005). How to study proteins by circular dichroism. *Biochim. Biophys. Acta Proteins Proteom.* **1751**, 119–139.

Ling, S.J., Qi, Z.M., Knight, D.P., Shao, Z.Z., and Chen, X. (2011). Synchrotron FTIR microspectroscopy of single natural silk fibers. *Biomacromolecules* **12**, 3344–3349.

Marchesano, V., Hernandez, Y., Salvenmoser, W., Ambrosone, A., Tino, A., Hobmayer, B., M De La Fuente, J., and Tortiglione, C. (2013). Imaging inward and outward trafficking of gold nanoparticles in whole animals. *ACS Nano* **7**, 2431–2442.

McNamara, M.C., Sharifi, F., Wrede, A.H., Kimlinger, D.F., Thomas, D.G., Vander Wiel, J.B., Chen, Y.F., Montazami, R., and Hashemi, N.N. (2017). Microfibers as physiologically relevant platforms for creation of 3D cell cultures. *Macromol. Biosci.* **17**, 10.

Miller, L.M., Bourassa, M.W., and Smith, R.J. (2013). FTIR spectroscopic imaging of protein aggregation in living cells. *Biochim. Biophys. Acta* **1828**, 2339–2346.

Moros, M., Kyriazi, M.E., El-Sagheer, A.H., Brown, T., Tortiglione, C., and Kanaras, A.G. (2018). DNA-coated gold nanoparticles for the detection of mRNA in live *Hydra vulgaris* animals. *ACS Appl. Mater. Interfaces* **11**, 13905–13911.

Palama, I., Di Maria, F., Viola, I., Fabiano, E., Gigli, G., Bettini, C., and Barbarella, G. (2011). Live-cell-permeant thiophene fluorophores and cell-mediated formation of fluorescent fibrils. *J. Am. Chem. Soc.* **133**, 17777–17785.

Obrig, T.G., Culp, W.J., Mckeehan, W.L., and Hardesty, B. (1971). The mechanism by which cycloheximide and related glutarimide antibiotics inhibit peptide synthesis on reticulocyte ribosomes. *J. Biol. Chem.* **246**, 174–181.

Palama, I.E., Di Maria, F., D'amone, S., Barbarella, G., and Gigli, G. (2015). Biocompatible and biodegradable fluorescent microfibers physiologically secreted by live cells upon spontaneous uptake of thiophene fluorophore. *J. Mater. Chem. B* **3**, 151–158.

Rea, I., Terracciano, M., Chandrasekaran, S., Voelcker, N.H., Dardano, P., Martucci, N.M., Lamberti, A., and De Stefano, L. (2016). Bioengineered silicon diatoms: adding photonic features to a nanostructured semiconductive material for biomolecular sensing. *Nanoscale Res. Lett.* **11**, 405.

Rising, A., and Johansson, J. (2015). Toward spinning artificial spider silk. *Nat. Chem. Biol.* **11**, 309–315.

Stavrindou, E., Gabrielsson, R., Gomez, E., Crispin, X., Nilsson, O., Simon, D.T., and Berggren, M. (2015). Electronic plants. *Sci. Adv.* **1**, e1501136.

Stavrindou, E., Gabrielsson, R., Nilsson, K.P., Singh, S.K., Franco-Gonzalez, J.F., Volkov, A.V., Jonsson, M.P., Grimoldi, A., Elgland, M., Zozoulenko, I.V., et al. (2017). In vivo polymerization and manufacturing of wires and supercapacitors in plants. *Proc. Natl. Acad. Sci. U S A* **114**, 2807–2812.

Tortiglione, C., Antognazza, M.R., Tino, A., Bossio, C., Marchesano, V., Bauduin, A., Zangoli, M., Morata, S.V., and Lanzani, G. (2017). Semiconducting polymers are light nanotransducers in eyeless animals. *Sci. Adv.* **3**, e1601699.

Tortiglione, C., Quarta, A., Malvindi, M.A., Tino, A., and Pellegrino, T. (2009). Fluorescent nanocrystals reveal regulated portals of entry into and between the cells of *Hydra*. *PLoS One* **4**, e7698.

Viola, I., Palama, I.E., Coluccia, A.M.L., Biasiucci, M., Dozza, B., Lucarelli, E., Di Maria, F., Barbarella, G., and Gigli, G. (2013). Physiological formation of fluorescent and conductive protein microfibers in live fibroblasts upon spontaneous uptake of biocompatible fluorophores. *Integr. Biol.* **5**, 1057–1066.

Wagner, C.D., Allison, J.W., Rumble, J.R., Jr, and Powell, C.J. (1997). SRD-20 X-ray Photoelectron Spectroscopy Database. (version 2.0) (Gaithersburg, MD: National Institute of Standards and Technology (NIST)).

Xu, Z.P., Shi, L.Y., Yang, M.Y., Zhang, H.P., and Zhu, L.J. (2015). Fabrication of a novel blended membrane with chitosan and silk microfibers for wound healing: characterization, in vitro and in vivo studies. *J. Mater. Chem. B* **3**, 3634–3642.

Zhang, D., Qi, G.B., Zhao, Y.X., Qiao, S.L., Yang, C., and Wang, H. (2015). In situ formation of nanofibers from purpurin18-peptide conjugates and the assembly induced retention effect in tumor sites. *Adv. Mater.* **27**, 6125–6130.

Zhao, M.Z., Cheng, D.B., Shang, Z.R., Wang, L., Qiao, Z.Y., Zhang, J.P., and Wang, H. (2018). An “in vivo self-assembly” strategy for constructing superstructures for biomedical applications. *Chin. J. Polym. Sci.* **36**, 1103–1113.

iScience, Volume 23

## **Supplemental Information**

### ***In Vivo* Bioengineering of Fluorescent**

### **Conductive Protein-Dye Microfibers**

**Maria Moros, Francesca Di Maria, Principia Dardano, Giuseppina Tommasini, Hiram Castillo-Michel, Alessandro Kovtun, Mattia Zangoli, Martina Blasio, Luca De Stefano, Angela Tino, Giovanna Barbarella, and Claudia Tortiglione**

## Supplemental information

Scheme S1. Molecular structures of DTTO, compound 2 and compound 3

Figure S1. Toxicological evaluation of DTTO and ECB04 in *Hydra vulgaris*: chronic condition

Figure S2. Toxicological evaluation of DTTO in *Hydra vulgaris*: acute condition

Figure S3. *In vivo* and *in vitro* toxicological evaluation of DTTO in *Hydra*

Figure S4. Biofiber production is specifically induced by DTTO and not by other oligothiophene-based fluorophores

Figure S5. Effect of green emitting thiophene-based compound 2 and compound 3 on *Hydra* tissue and cells

Figure S6. Imaging DTTO-based biofibers on *Hydra* tentacle

Figure S7. Structural and optical differences between DTTO aggregates and biofibers

Figure S8. Biofiber efficiency of production and yield are related to the DTTO concentration and time post treatment.

Figure S9. Biofiber formation is prevented by the protein synthesis inhibitor cycloheximide

Figure S10. Morphological, electrical and optical characterization of biofibers and DTTO aggregates

Table S1. Statistical comparisons relative to the graph of Figure 1K

Table S2. Atomic concentration of elements in biofibers

## Supplemental video

Movie S1- Detail of biofibers located on *Hydra* tentacles

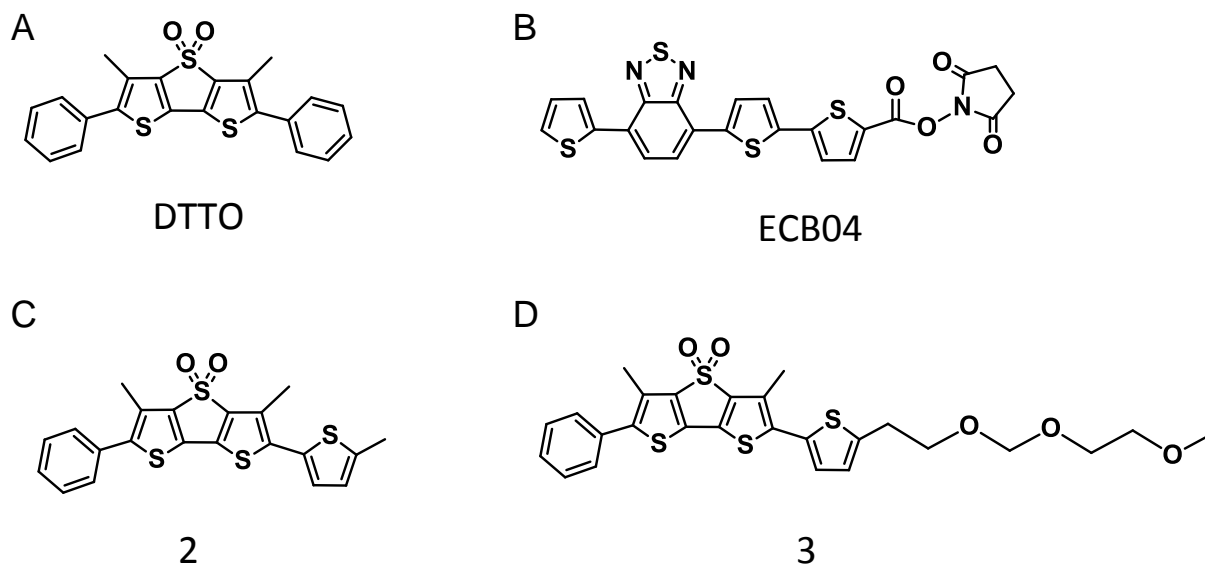
Movie S2- Green fluorescent biofibers located on two *Hydra* tentacles

## Transparent methods

## Supplemental References

## Synthesis and characterization of DTTO and other thiophene based fluorophores

For DTTO (Scheme 1) the synthetic details, NMR and optical characterizations have been previously reported. (Palama et al., 2011) The control fluorophores ECB04, compound 2 and compound 3, have also been previously characterized (Palama et al., 2011).



**Scheme S1. Molecular structure of thiophene based fluorophores. Related to Figure 1, Figure S1, Figure S4, and Figure S5.**

Molecular structure of **(A)** the green fluorescent semiconducting dye DTTO **(B)** the red emitting ECB04 (2,5-dioxopyrrolidin-1-yl-5'-(7-(thiophen-2-yl)benzo[c][1,2,5]thiadiazol-4-yl)-[2,2'-bithiophene]-5-carboxylate. **(C)** Compound 2: [2-phenyl-6-(2-methylthiophene)-3,5-dimethyl-dithieno[3,2-b:2',3'-d]thiophene-4,4-dioxide]. **(D)** Compound 3: [2-phenyl-6-(2-(2-((2-methoxyethoxy)methoxy)ethyl)thiophene)-3,5-dimethyl-dithieno[3,2-b:2',3'-d]thiophene-4,4-dioxide]

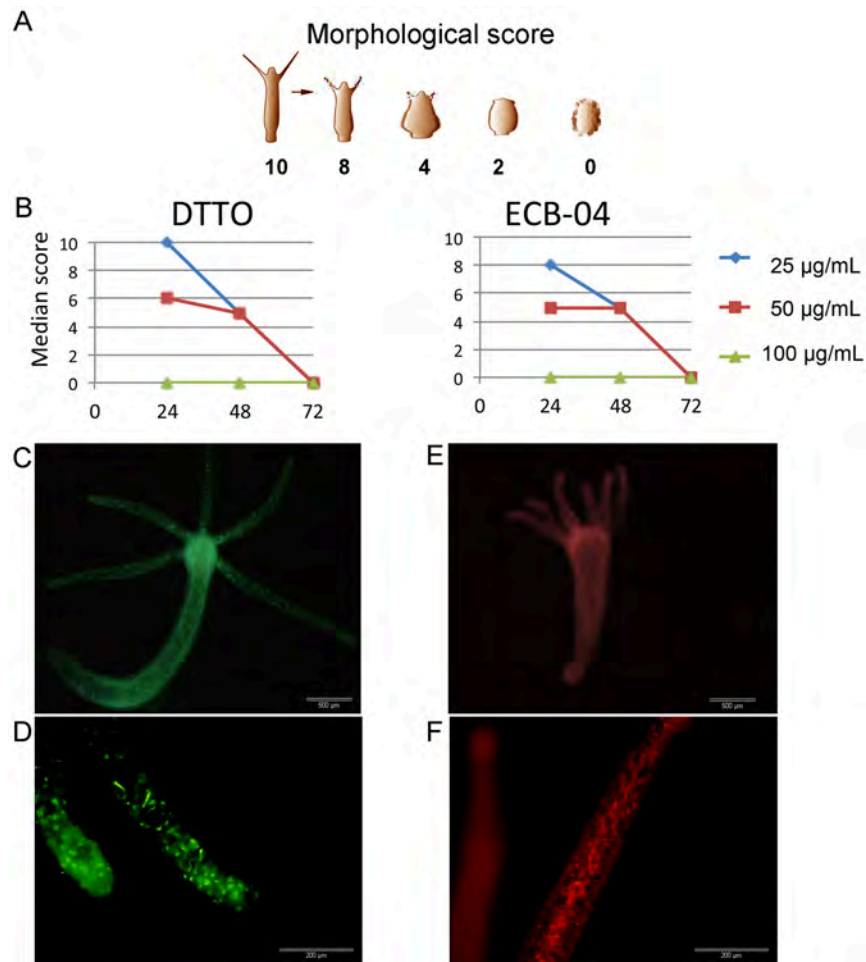


**Figure S1. Toxicological evaluation of DTTO and ECB04 in *Hydra vulgaris*: chronic condition. Related to Figure 1**

(A) The scheme shows progressive morphological alterations induced by the presence of a toxicant in the medium bathing living animals. The methodology is reported in the Transparent method section. (B) The graphs show the dose responses curve for DTTO and ECB04 (N=20). The median score value is reported as function of the incubation time. Compared to DTTO, ECB04 was slightly toxic, as indicated by the lower median score values at 24 h. (C) *In vivo* fluorescence imaging of a whole animal incubated with DTTO (25 µg/ml) for 24 h. (D) Detail of the tentacles, showing long fluorescent fibers. (E) *In vivo* fluorescence imaging of a whole animal incubated with ECB04 (25 µg/ml) for 24 h. The contracted shape shows the slight toxicity. (F) A detail of a tentacle shows the absence of biofiber production. Scale bars, 500 µm in C, E, 200 µm in D, F.

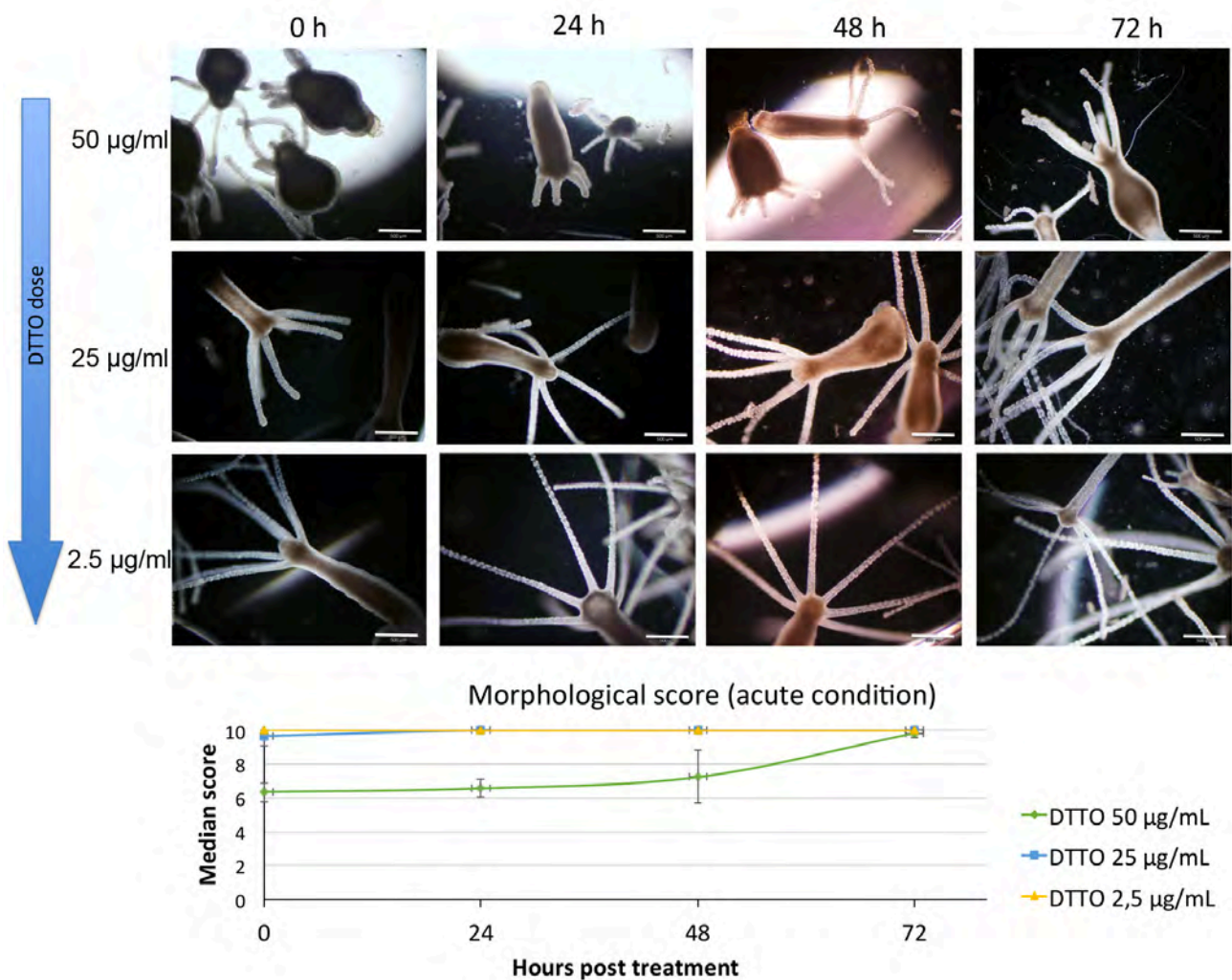


**Figure S2. Toxicological evaluation of DTTO in *Hydra vulgaris*: acute condition. Related to Figure 1**

Polyps were treated 5 h with DTTO at the indicated concentrations and observed at 24 h intervals post treatment. Data show biosafety of 2.5 and 25 µg/ml doses, while at  $t= 0$  h,  $t= 24$  h and  $t= 48$  h post treatment animal contraction and tentacle shortening were observed, indicating a slight effect of DTTO, completely recovered at 72 h time point. Morphological scores are same as in Figure S1, ranging from 10 (healthy animal) to zero (disintegrated animal). Scale bars: 500 µm. The quantitative estimation of these toxicological traits are reported in the graph below, showing the median scores monitored on  $n= 60$  polyps at each time point. Data represent the average of three independent experiments  $\pm$  SD.

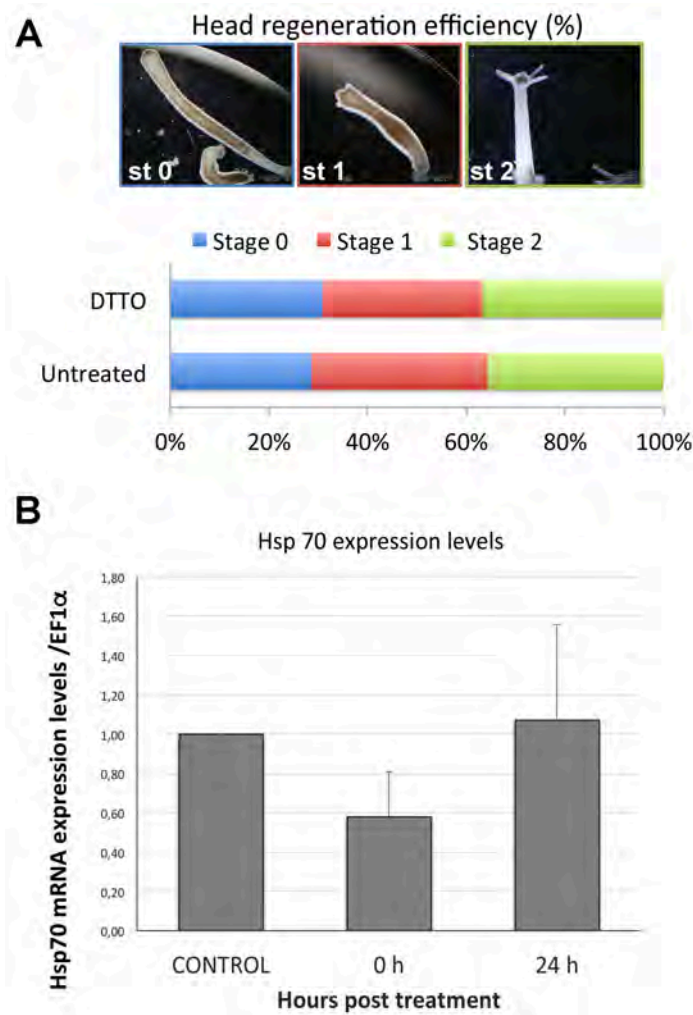


**Figure S3. *In vivo* and *in vitro* toxicological evaluations of DTTO in *Hydra*. Related to Figure 1**

**(A)** Impact of DTTO on regenerative capability of *Hydra*. The methodology is reported in the Transparent method section. Briefly, groups of 20 polyps were treated 5 h with DTTO 25  $\mu\text{g}/\text{mL}$ , and after washing bisected and allowed to regenerate in fresh medium. After 24 h all polyps show wound closure and not differences between treated and untreated polyps. The graph shows the average distribution of all developmental stages, from three biological replica ( $n=60$ ), at 48 h post amputation. No differences were detected between DTTO treated and untreated polyps. **(B)** Expression pattern of *Hsp70* stress responsive gene in DTTO treated polyps by qRT-PCR analysis using Elongation factor 1-alpha (*Ef-1 $\alpha$* ) as reference gene. Groups of 20 *Hydra* were treated 5 h with DTTO 25  $\mu\text{g}/\text{mL}$ , then washed, and after 24 h processed for qRT-PCR. Not significant differences were detected between treated and untreated animals. Statistical comparisons were performed using one sample t test.

List of primers employed for qRT-PCR

gene	accession number	Forward primer	reverse primer
<i>Ef-1a</i>	XP_012553476.1	ccaggagacaatgtcggttt	gcttcaatggcaggatcatt
<i>Hsp70.1</i>	XP_002159813	cgacgtattcagacaatcaacc	caatttgaggacacctctgg

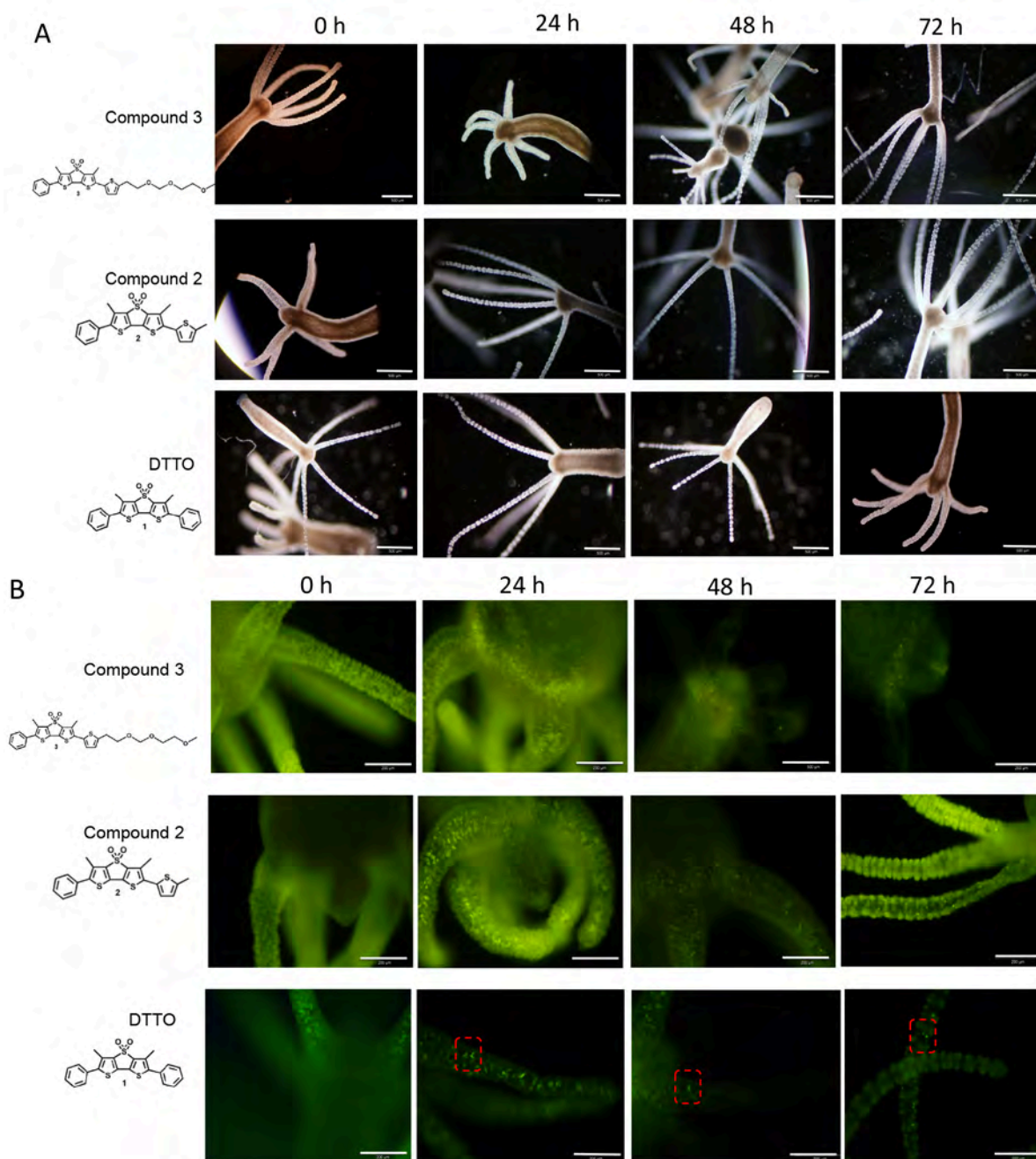


**Figure S4. Biofiber production is specifically induced by DTTO and not by other oligothiophene-based fluorophores. Related to Figure 1**

Group of 20 polyps were soaked for 5 h with the indicated fluorophore (time zero) and after washing monitored by fluorescence microscopy every 24 h. **(A)** Brightfield images show the absence of evident toxic effects induced by any fluorophores, as indicated by normal polyp morphology and behavior. Scale bars, 500  $\mu\text{m}$ . **(B)** Fluorescence microscopy images of the same polyps showing the presence of biofibers from 24 h time point onwards only on tentacles from the DTTO treated polyps (framed by red dotted squares). Scale bars, 200  $\mu\text{m}$ .

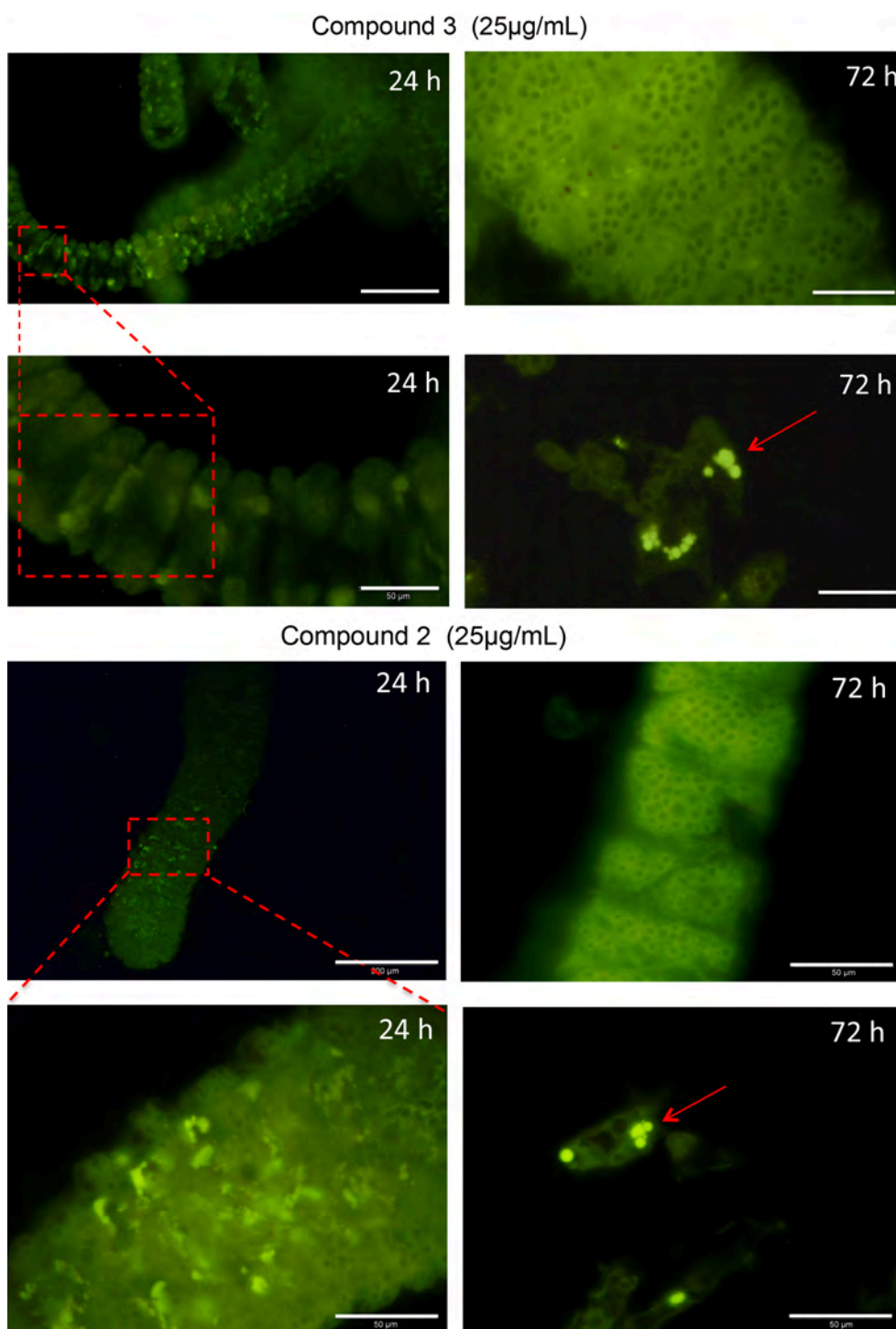


**Figure S5. Effect of green emitting thiophene-based compound 2 and compound 3 on *Hydra* tissue and cells. Related to Figure 2**

Treatment of polyps with compound 2 and 3 at the same doses and time as DTTO does not induce biofiber production. Animal tissues show diffuse fluorescence both at 24 h and 72 h post treatment. Detail of red square framed regions of the tentacles at 24 h time point are shown at higher magnification below. Single cells suspension prepared at 72 h by maceration of treated animals (see method section) show dye accumulation into cells (red arrows). Scale bars, 100  $\mu$ m upper left images; 50  $\mu$ m all others.

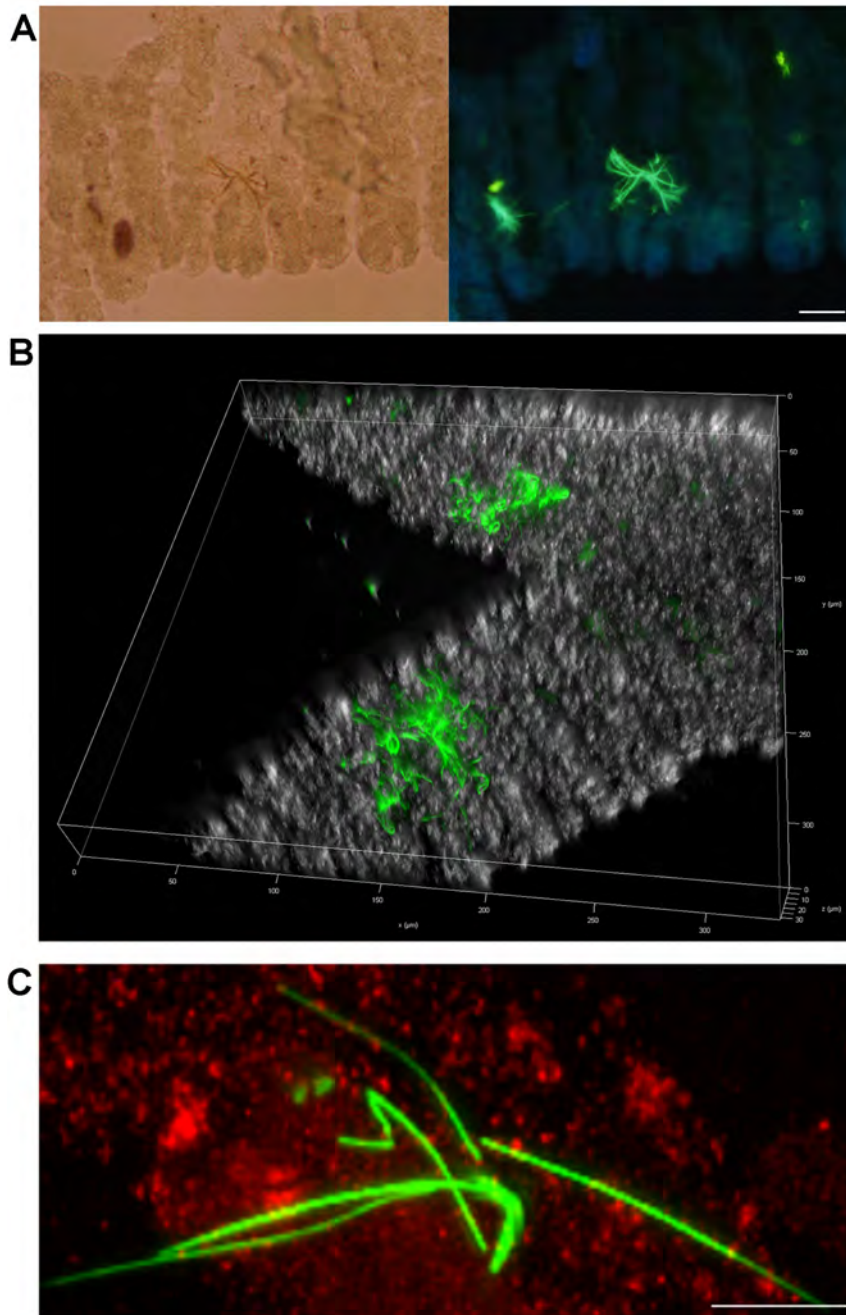


**Figure S6. Imaging DTTO-based biofibers on *Hydra* tentacle. Related to Figure 1, Movie S1 and Movie S2**

**(A)** Bright field (left) and fluorescence imaging (right) of a *Hydra* tentacle prepared by maceration from DTTO treated polyps. After 5 h incubation with 25  $\mu\text{g}/\text{ml}$  DTTO, polyps were washed and left in fresh Hydra medium for 24 h. Polyps were then relaxed in 2% urethane, soaked over night into maceration solution (glycerol: acidic acid: water= 1:1:13) and fixed with 4% paraformaldehyde. Macerated cells and piece of tissues were spread on glass slide and analysed by optical microscopy. Fluorescent biofibers showing different morphologies were easily detected on the external surface of the tentacles. Scale bar, 10  $\mu\text{m}$ . **(B)** Bright field and fluorescence optical merged images of *Hydra* tentacles. After 5 h incubation with 25 mg/ml DTTO, whole polyps were washed and left in fresh Hydra medium for 24 h. After relaxing in 2% urethane, polyps were fixed with 4% paraformaldehyde and mounted on microscopy slide. Image was obtained by using a Leica THUNDER Imager 3D Cell Culture microscope, 40x dry objective, NA=0.95. **(C)** Maximum Intensity Projection of the fluorescence Immunolocalization performed on *Hydra* macerates.

Immunolocalization was performed on macerates from DTTO treated Hydra using *Hydra* anti-collagen I. The methodology is reported in the Transparent method section. The image shows a green emitting fiber on the top of a cell. Cross-reaction with Hydra anti-collagen I is evident on the cell laying below the biofiber (red), but there are not clear signs of co-localization on the fiber. This may be due to the absence of Hydra collagen I inside the fibers, or to technical limits. The maceration procedure, the structural masking of the epitope due to DTTO bonding or the complexation may also prevent the cross reaction. Scale bar, 10  $\mu\text{m}$

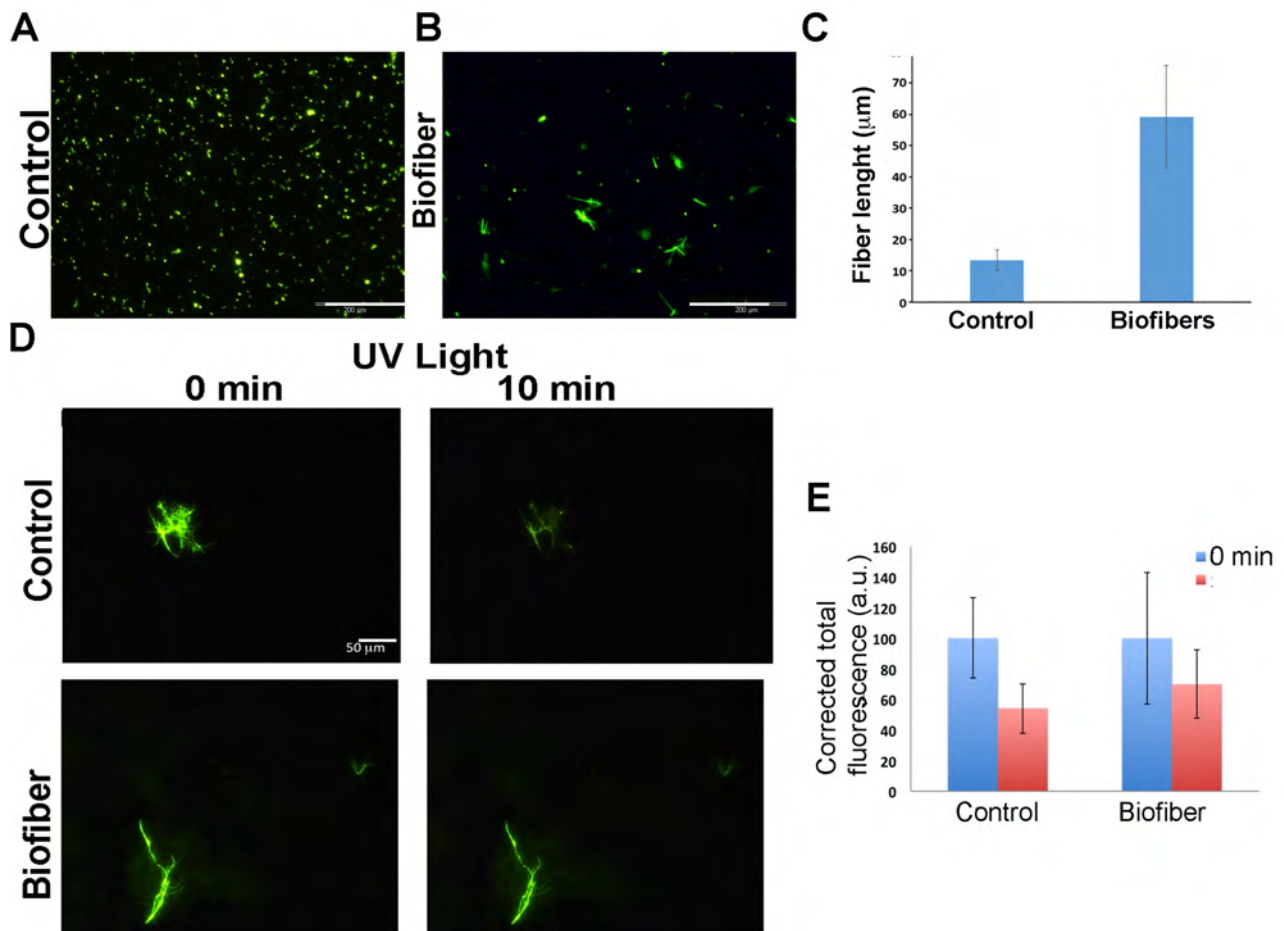


**Figure S7. Structural and optical differences between DTTO aggregates and biofibers. Related to Figure 2.**

(A) Spontaneous aggregates formed by DTTO in Hydra medium and (B) Biofibers produced by animals treated with DTTO for 5 h. (C) While the DTTO in solution formed small aggregates of 13.3  $\mu\text{m}$  mean average length, the biofibers synthesized by the polyps present a mean length of 59.13  $\mu\text{m}$ . Scale bars, 200  $\mu\text{m}$ . (D-E) Photobehaviour of biofibers and DTTO aggregates. Aggregates formed from DTTO in Hydra medium (control) and biofibers produced by the animals were exposed to UV light for 10 min and the fluorescence intensity recorded using different regions of interest (ROI), before and after the illumination. DTTO aggregates lost 45.8 % of their initial fluorescence, while biofibers lost only 30.1%. Data represent the average from three independent experiments. Statistical comparisons were performed using one sample t test.

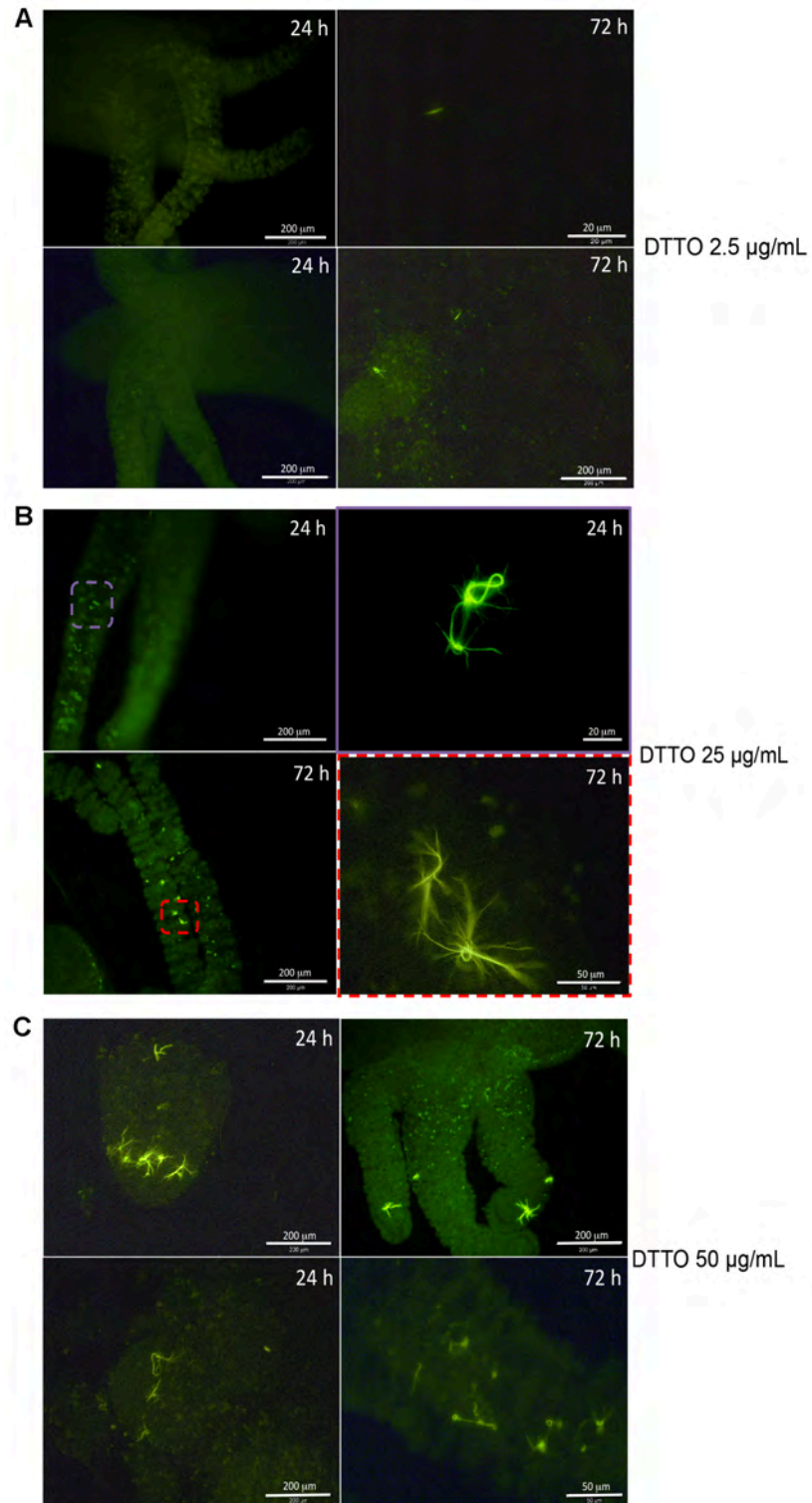


**Figure S8. Biofiber efficiency of production and yield are related to the DTTO concentration and time post treatment. Related to Figure 1.**

By increasing the DTTO concentration (2.5 to 50 µg/ml) and incubation period post treatment (24 to 72 hours) the average number of animals producing biofiber increases, although a high variability was found between individuals. Scale bars are indicated in each image.

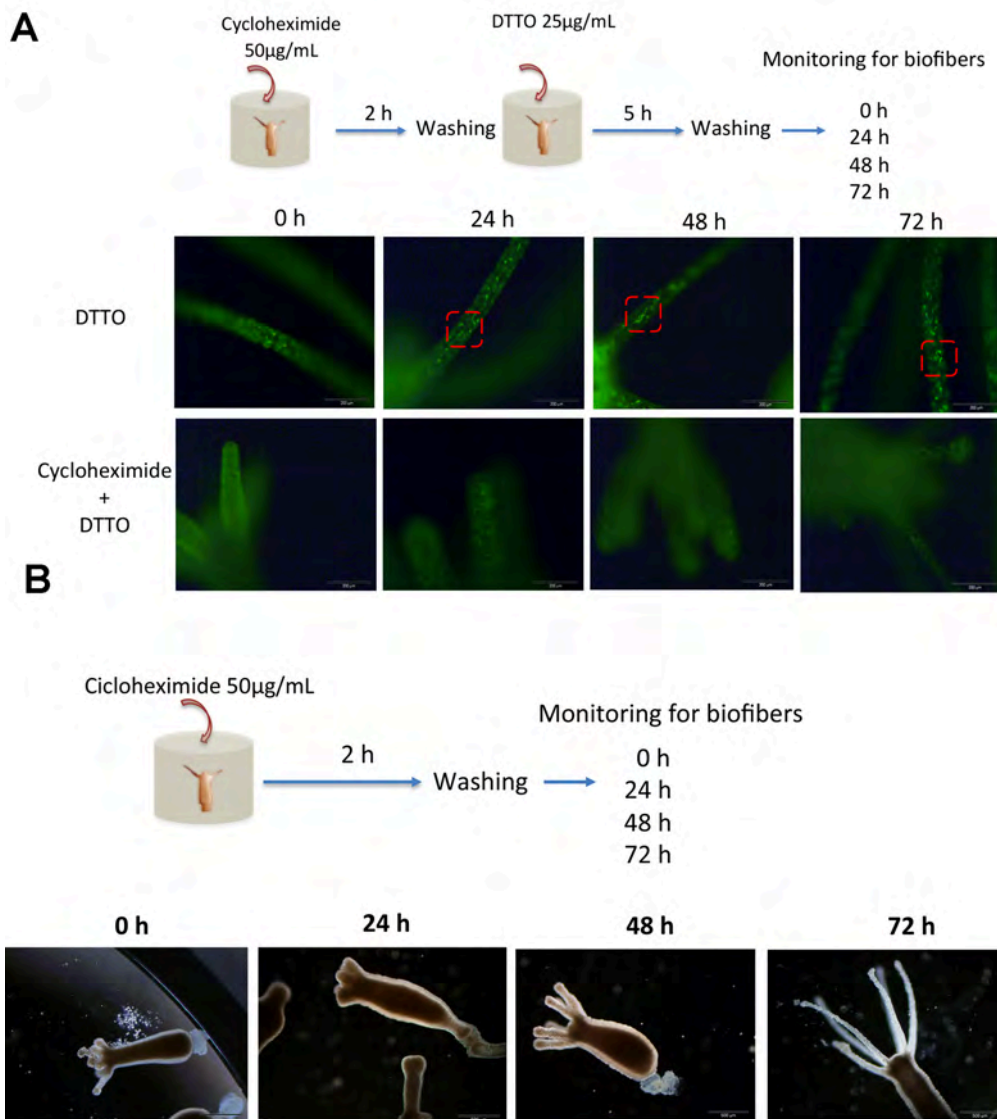


**Figure S9. Biofiber formation is prevented by the protein synthesis inhibitor cycloheximide. Related to Figure 1**

**(A)** Cycloheximide is an inhibitor of protein biosynthesis and broadly used in cell biology in terms of determining the half-life of a given protein (Kao et al., 2015, Obrig, 1971). The scheme of the experiment is shown in the upper panel. *Hydra* treated with cycloheximide (Sigma-Aldrich) only rarely produce biofibers (see Figure 1), indicating that an active process of protein synthesis is involved in biofiber production. Experiments were performed in triplicate on a total of 50 polyps. Representative polyps are shown in the images. Scale bars, 500  $\mu\text{m}$  (upper images) and 200  $\mu\text{m}$  (lower). **(B)** Evaluation of cycloheximide biocompatibility in *Hydra vulgaris*. Polyps were treated with cycloheximide 50  $\mu\text{g}/\text{mL}$  for 2 h and polyp morphology monitored every 24 h intervals. Images show that after washing the animal morphology is rapidly recovered, indicating good biocompatibility for this drug in *Hydra*.

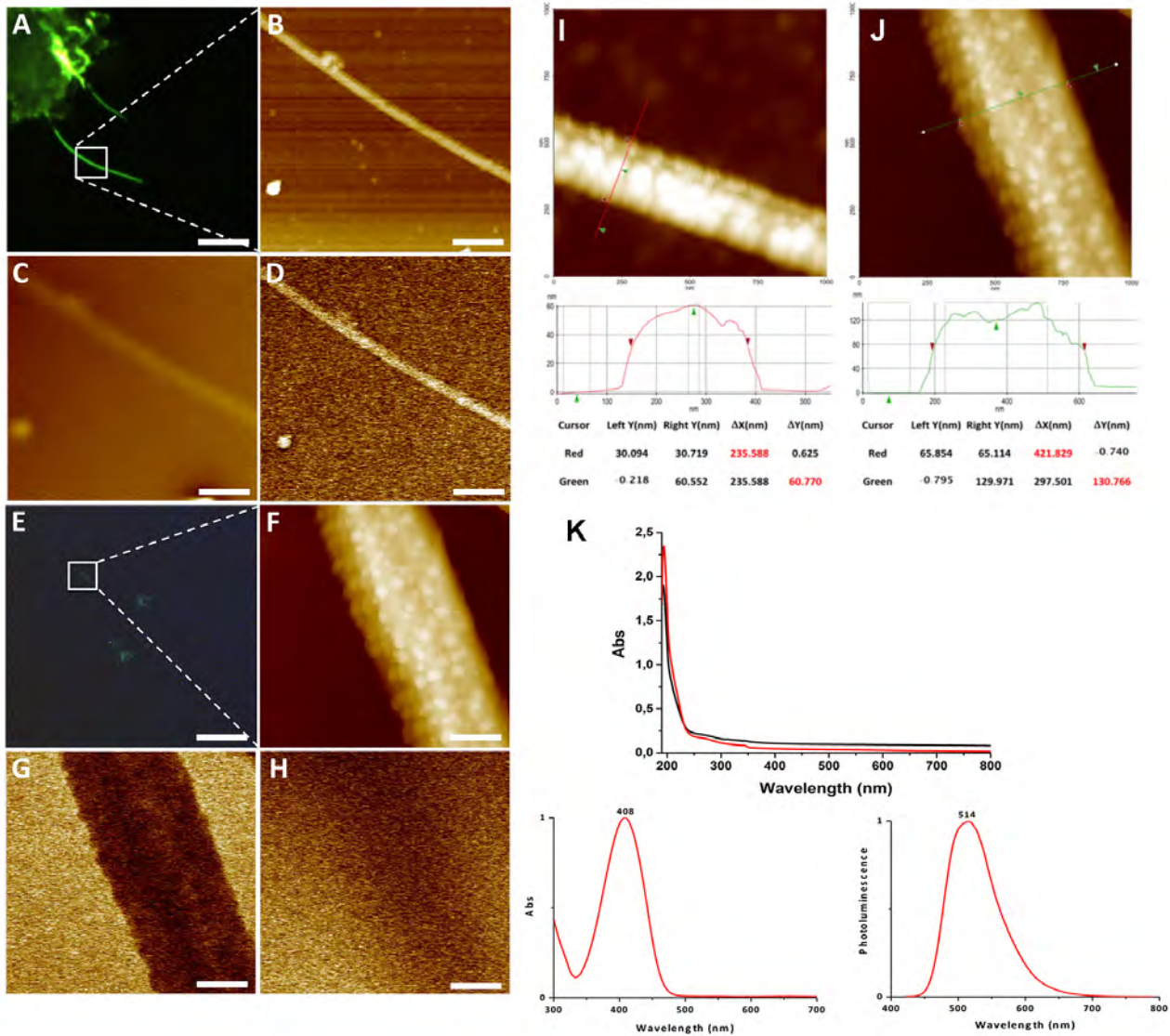


**Figure S10. Electrical, morphological, and optical characterization of biofibers and DTTO aggregates. Related to Figure 3 and Figure 5**

(A) Fluorescence image of a biofiber (scale bar, 50  $\mu\text{m}$ ). The white square shows the sub-region selected for AFM and EFM characterizations. (B) AFM topography (scale bar, 2  $\mu\text{m}$ ). EFM amplitude of the biofiber at bias voltage. (C) 0 V and (D) -10 V, respectively (scale bars, 2  $\mu\text{m}$ ). (E) Fluorescence image of a DTTO self-aggregated fragment (scale bar, 20  $\mu\text{m}$ ). The white square shows the sub-region selected for AFM and EFM characterizations. (F) AFM topography (scale bar, 200 nm). EFM amplitude of the control at bias voltage (G) 0 V and (H) -10 V, respectively (scale bars, 200 nm). (I-K) Characterization of biofibers and DTTO aggregates. AFM topography images on 1x1 mm<sup>2</sup> field, at 512x512 pixels resolution of (I) a biofiber produced in *Hydra* and (J) control, DTTO spontaneously aggregated in *Hydra* medium. Images are presented and analyzed on a line perpendicular to fiber direction. The height measurements on the lines are reported in the corresponding graphs and tables. (K) Optical characterization of macerates and DTTO aggregates. Upper panel: spectra of macerates from DTTO treated *Hydra* (black line) and untreated *Hydra* (red line). Lower: absorption and emission spectra of DTTO in methylene chloride

Time	DTTO [ $\mu\text{g/mL}$ ]	P value	Significance
24 h	2.5 vs 25	0.0017	**
24 h	2.5 vs 50	< 0.0001	***
24 h	25 vs 50	0.0093	**
24 h	25 vs 25 (cyclohex.)	0.0018	**
72 h	2.5 vs 25	< 0.0001	***
72 h	2.5 vs 50	< 0.0001	***
72 h	25 vs 50	< 0.0001	***
72 h	25 vs 25 (cyclohex.)	< 0.0001	***
24 h vs 72 h	50	0.0037	**
24 h vs 72 h	25	0.9107	Not significant
24 h vs 72 h	2.5	0.2045	Not significant
24 h vs 72 h	25 (cyclohex.)	0.2839	Not significant

**Table S1. Statistical comparisons relative to the graph of Figure 1K. Related to Figure 1**

Statistical comparisons were performed using unpaired t-test; \*,  $P < 0.05$ ; \*\*,  $P < 0.01$ ; \*\*\*,  $P < 0.001$ .

Transition	S 2p		N 1s	P 2p	C 1s	O 1s	Au 4f
Chemical state	S-C	S=O	N-C	P-O	C-C/C-N	Mixed	Au <sup>0</sup>
<b>Au</b>	-	-	-	-	11.0±0.5	-	89.0±0.9
<b>DTTO/Au</b>	5.9±0.5	3.4±0.4	-	-	74.8±0.9	8.1±0.5	8.0±0.5
<b>Biofibers/Au</b>	0.13±0.05	0.12±0.05	5.1±0.5	1.7±0.2	70.6±0.9	15.7±0.7	6.2±0.5

**Table S2. Atomic concentration of elements in biofibers. Related to Figure 4.**

Atomic concentration of elements in Ar<sup>+</sup> sputtered Au, DTTO on Ar<sup>+</sup> sputtered Au and DTTO biofibers on Ar<sup>+</sup> sputtered Au. The Ar<sup>+</sup> sputtered Au presents no contamination from N, P, S or O. DTTO biofibers contains a c.a. 0.35% of Cl (Cl 2p signal).

## Transparent methods

### Animal Culture

*Hydra vulgaris* were asexually cultured in *Hydra* medium (1 mM CaCl<sub>2</sub>, 0.1 mM NaHCO<sub>3</sub>, pH=7). Animals were fed three times per week with freshly hatched *Artemia salina* nauplii at 18°C with a 12:12 h light: dark regime. Polyps from homogeneous populations without buds were selected for the experiments.

### Biofiber Production

DTTO, ECB04, compound 2 and compound 3 dyes were dissolved in the minimum amount of DMSO and then diluted in *Hydra* solution to obtain a stock solution. Chemical concentration to use for all experiments was selected based on previous reports performed in cell cultures (Viola et al., 2013), and here tested against *Hydra* in chronic or acute condition (see below).

In a typical experiment of biofiber formation 70 *Hydra* were treated with 1 mL of DTTO 25 µg/mL for 5 h in a plastic multiwell. Two control conditions were set up, *Hydra* cultured without DTTO, and DTTO in solution (25 µg/mL) without *Hydra* to characterize and differentiate fiber formation in presence or absence of animals. After incubation, all media were collected, polyps were extensively washed, maintained in 1 mL of fresh medium and continuously monitored up to 6 days post treatment by fluorescence microscopy (Nikon Eclipse Ti-E). The process of biofiber production was inhibited by the addition of Cycloheximide (Merk), a known inhibitor of the protein synthesis (Kao et al., 2015). *Hydra* polyps were pre-treated 2 h with cycloheximide (50 µg/mL) before DTTO addition, and biofiber production monitored for the following 72 h at 24 h intervals. Cycloheximide dose was selected on the bases of literature data on cell culture, where doses ranging from 50-300 µg/ml are recommended and incubation periods from 2 up to 24 h (Kao et al., 2015). We selected the lowest dose and treatment period and found biocompatibility for *Hydra* (Figure S9).

### Hydra Maceration into Fixed Single Cells

Polyps were macerated to obtain single-cell suspensions and to characterize the biofibers using a solution composed by acetic acid, glycerol and H<sub>2</sub>O in a 1:1:13 (v/v) ratio.(David, 1973) The obtained single-cell suspensions were fixed with 4% paraformaldehyde and spread on slides. After extensive washing in PBS (NaCl 137 mM, KCl 2.7 mM, Na<sub>2</sub>HPO<sub>4</sub> 10 mM, KH<sub>2</sub>PO<sub>4</sub> 1.8 mM) macerates were observed by an inverted microscope (Axiovert 100, Zeiss, JENA, GERMANY) equipped with a digital color camera (Olympus, DP70). The software system Cell F (Olympus) was used for imaging acquisition and analysis. For laser scanning confocal microscopy (LSCM) a Leica TCS SP5 microscope was used, equipped with a 100 oil immersion objective. Laser line at 488 nm for excitation was provided by an Ar laser.

In order to characterize the fibers by CD, UV-Vis, AFM and EFM, XPS and IMS the fiber content after maceration was enriched by centrifugation of the macerated suspension and water resuspension. Control samples containing DTTO in *Hydra* medium were also characterized using the same techniques.

### UV-Visible Spectroscopy and Circular Dichroism

The samples analysed were either cell macerates containing biofibers prepared from *Hydra* (sample A) or control samples, including DTTO in methylene chloride (sample B) or DTTO in *Hydra* solution (sample C). UV-Vis and PL data were obtained using a Perkin Elmer Lambda 20 spectrometer and a Perkin Elmer LS50 spectrofluorometer, respectively. Lifetime measurements were performed with the time correlated single photon counting accessory of Fluoromax-4 using 455 nm pulsed excitation (1 MHz repetition rate). CD spectra were collected using a spectropolarimeter JASCO J-715 under ambient conditions.

### Atomic Force Microscopy

Atomic and Electrostatic Force Microscopy imaging were performed with XE-100 AFM (Park Systems) and Lock-in Amplifier (SR-830) to distinguish electric force and Van der Waals force effect and obtain 3D images of fiber surfaces. Non-contact mode (NCM) was realized by oscillating metallic-silicon tips mounted on gold coated cantilevers 150 µm long with nominal resonance frequency 140-150 kHz and force constant of 7.4 N/m (PPP-NCSTAu, Park Systems). In EFM measurements an AC signal  $V(t)=V_0\sin(\omega t)+V_b$  was applied to the tip using Lock-in Amplifier, where  $V_0 = 2$  V and  $\omega = 17$  kHz and  $V_b$  was the bias voltage and was 0V, -10 V

and +10 V. Fixed cells obtained by maceration of DTTO treated animals were deposited on a gold-coated substrate in order to obtain a good conductivity of the background. As control a solution containing DTTO in Hydra medium was used. The sample preparation followed the procedure previously reported.(Cicatiello et al., 2017)(Oliviero et al., 2017) Briefly, 5 mL aliquots of the sample/imaging buffer were directly deposited by casting onto the substrate; after 2 min, samples were gently washed with deionized water in order to remove cell and salt traces, then, dried by evaporation at room temperature under a ventilated fume hood. Fluorescent fibrils were individuated by means of fluorescence microscopy (Leica Z16 APO fluorescence microscope equipped with a Leica camera DFC320; filter sets: 450–490 nm band-pass excitation filter, a 510 nm dichromatic mirror and a 515 nm suppression filter) and then the same imaging field was analysed by AFM and EFM. The images of AFM topography and EFM amplitude have 512x512 pixel resolution and the scan frequency was typically 0.5 Hz per line. When necessary, the AFM images were processed by flattening, to remove the background slope, and to adjust the contrast and brightness.

#### **Fourier Transform Infrared Micro-Spectroscopy (IMS)**

IMS analyses were performed at beamline ID-21 at the European Synchrotron Radiation Facility (ESRF) in Grenoble, France. The beamline is equipped with a Thermo Nicolet Continuum (Thermo Scientific, Madison, WI, U.S.A.) microscope coupled to a Thermo Nicolet Nexus FTIR spectrometer (Thermo Scientific, Madison, WI, U.S.A) with a 32X objective, a motorized sample stage, and a liquid nitrogen-cooled 50  $\mu\text{m}$  mercury cadmium telluride detector. Samples were mounted on  $\text{BaF}_2$  windows (0.4 mm thick) and observed at 10x magnification using a UV illuminator to locate the fibers. After, a point outside the fiber was selected as background and a region was marked to perform mapping at 5  $\mu\text{m}$  step size adding 64 scans with a resolution of 6  $\text{cm}^{-1}$ . From this hyperspectral data set, a distribution map of amide I (1650  $\text{cm}^{-1}$  C=O stretching vibration of the peptide bond with a minor contribution from C-N stretching vibration) was obtained after processing the spectra to second derivative (Savitzky-Golay 21 point filter and second order polynomial) and plotting the intensity at 1655  $\text{cm}^{-1}$ . From this map 12 and 15 spectra were extracted from the fiber zone and outside, respectively. The spectra from each were averaged and plotted to observe the main changes in the region 1500-1800  $\text{cm}^{-1}$  looking for the characteristic absorption bands of protein secondary structure amide I and amide II (Benseny-Cases et al., 2014).

#### **X-ray Photoelectron Spectroscopy Measurements (XPS)**

XPS spectra were obtained using a Phoibos 100 hemispherical energy analyser (Specs GmbH, Berlin, Germany) and Mg Ka radiation ( $\hbar\omega$  1253.6 eV; power = 125W) in constant analyser energy (CAE) mode, with analyser pass energy of 40 eV. The overall resolution of 1.5 eV was measured and analyser was calibrated by using the Ag 3d 5/2 (368.3 eV) signals from freshly  $\text{Ar}^+$  sputtered samples. Charging effects was corrected by calibration of Binding Energy on C 1s (285.5 eV) for all spectra. Base pressure in the analysis chamber during analysis was  $2 \cdot 10^{-9}$  mbar. Data analysis and fit were performed with CasaXPS software, after Shirley background subtraction, S 2p and P 2p doublets were fitted by constant spin-orbit split ( $2p_{1/2}$ - $2p_{3/2}$ ) of 1.18 eV and 0.86 eV respectively. More detail about instrumental configuration and data analysis can be found in a previous report (Kovtun, 2019) . Both samples were deposited on golden slides purchased from Arrandee (Germany) having an Au thickness of 250 nm and a Cr adhesive layer of 2.5 nm. Before deposition gold substrates were cleaned by 5 min acetone sonic bath and 5 min isopropanol sonic bath; slides were dried by using a  $\text{N}_2$  gas flow. Part of organic impurities were removed by 5 min air plasma treatment (Diener, Germany). The last impurities were removed by  $\text{Ar}^+$  ion sputtering in Ultra High Vacuum conditions. The obtained Au slides present no S, O, N, P contamination. Samples were prepared by drop-casting the solutions on freshly cleaned golden slice and blowing of pure  $\text{N}_2$  for few minutes.

## **Method for Immunofluorescence on *Hydra* macerates**

*Hydra* macerates (as described above) were spread on slides, washed thrice for 5 min with PBS, and permeabilized with PBS 0,1% tween (PBST) for 1 h. After washing with PBS, samples were blocked 2 h with 5% BSA in PBST, and *Hydra* anti-collagen I antibody (kindly provided by M. Isas, University of Chicago) was added at 1:250 dilution in PBST-BSA and incubated over night at 4°C. Following washes (5x for 5 min) the red emitting alexa-594 donkey anti-mouse secondary antibody was used to detect cross-reacting collagen I proteins on biofibers. After 2 h incubation, samples were washed with PBST and mounted on a coverslip. Samples were scanned using a CLSM, and z stacks acquired every 0.125 mm. Maximum Intensity Projection was obtained using the microscope software.

## **Toxicological evaluation and determination of the test dose**

### **1) DTTO toxicity evaluation: chronic condition**

*Hydra* is highly sensitive to organic and inorganic compounds and several approaches may be used to determinate the impact of any medium suspended compound on its physiology, i.e. morphology, reproduction rate, regeneration efficiency. As straightforward toxicological endpoint, we monitored the animal morphology in response to increasing dose of DTTO and exposure time. We used a toxicity test based on numerical scores to describe morphological alteration, adapted by our group from a previously described method used to assess the toxic effect of organic compounds on *Hydra* (Allocca et al., 2019, Ambrosone et al., 2012, Ambrosone and Tortiglione, 2013, Ambrosone et al., 2017, Karntanut and Pascoe, 2002, Wilby and Tesh, 1990). After addition of a test compound to the medium bathing living animals, the morphology is observed and a numerical score assigned to each specimen, from 10 (healthy animal) to zero (disintegrated animal). For DTTO and ECB04 dose-response curves were determined in the range of 25-100 µg/mL in chronic condition from 24 h up to 72 h.

### **2) DTTO toxicity evaluation: acute condition**

A detailed toxicological analysis was performed by assessing several toxicological endpoints, i.e. the impact of DTTO on animal morphology, the efficiency of regeneration and the expression level of a stress responsive gene.

#### - Impact on morphology

Group of 20 animals were treated for a fixed period of time (5 h) to increasing concentrations (2.5 µg/ml, 25 µg/ml and 50 µg/ml) of DTTO, then washed and inspected by optical microscopy at regular intervals (Figure S2). Morphological changes were detected only at the higher dose tested, and persisted up to 48 h post treatment, recovering the normal physiology at 72 h. These data indicate that DTTO is well tolerated up to 25 µg/ml, while higher doses may slightly impact on the animal viability early after treatment.

#### - Impact on regeneration efficiency

*Hydra* possesses a unique potential to regenerate missing body parts upon amputation (Galliot et al., 2006, Bode, 2003, Holstein et al., 2003). This tightly controlled phenomenon can be impaired by the presence of toxicants into the medium (Wilby and Tesh, 1990). We have previously tested the impact of several nanocrystals on *Hydra* using this assay (Ambrosone et al., 2012, Allocca et al., 2019, Ambrosone et al., 2017) which together with the analysis of expression of stress responsive genes may provide useful clues on the toxicity of organic or inorganic compounds.

Groups of 20 *Hydra* were treated 5 h with DTTO 25 µg/mL, then washed, bisected and allowed to regenerate in fresh medium. Every 24 h developmental stages of all animals were recorded and compared to untreated animals, bisected at the same time. Results shown in Figure S3 A show not differences in the percentages of regenerating stages between the two sets of animals at 48 h post amputation (no. of polyps=60), suggesting that the DTTO treatment does not affect the regenerative capability of the polyps.

#### - Impact on stress responsive gene expression levels

Groups of 20 *Hydra* were treated 5 h with DTTO 25 µg/mL, then washed, and after 24 h processed for RNA extraction and quantitative real time polymerase chain reaction (qRT-PCR), using the methods previously described (Ambrosone et al., 2012), to analyze expression level of *Hsp70*. This family of proteins is considered a potent buffering system for cellular stress, either from extrinsic (physiological, viral and environmental) or intrinsic (replicative or oncogenic) stimuli (Murphy, 2013). As such, its deregulation is associated to impairment of protein homeostasis and is found in many types of cancers. The graph of

Figure S3 B shows not significant differences in the *Hsp70* mRNA expression levels between DTTO treated and untreated animals, suggesting that DTTO treatment does not cause cell stress, at least in the temporal window overlapping with biofiber production. A comprehensive molecular analysis of other genes involved in different metabolic pathways may help to identify the molecular mechanisms underlying DTTO induced biofiber production and may be object of future investigation.

### Statistical Analysis

Results of the assays were expressed as mean  $\pm$  standard deviation (s.d.) of three independent independent experiments. Statistical analysis was performed using the GraphPad Prism 7 software (GraphPad Software Inc., La Jolla, CA). The significance of differences was evaluated with unpaired Student's t test, with the level of significance set at probabilities of \*,  $P < 0.05$ ; \*\*,  $P < 0.01$ ; \*\*\*,  $P < 0.001$

### SUPPLEMENTAL REFERENCES

- Allocca, M., Mattera, L., Bauduin, A., Miedziak, B., Moros, M., De Trizio, L., Tino, A., Reiss, P., Ambrosone, A. & Tortiglione, C. 2019. An Integrated Multilevel Analysis Profiling Biosafety and Toxicity Induced by Indium- and Cadmium-Based Quantum Dots in Vivo. *Environ Sci Technol.* 53, 3938-3947.
- Ambrosone, A., Mattera, L., Marchesano, V., Quarta, A., Susha, A. S., Tino, A., Rogach, A. L. & Tortiglione, C. 2012. Mechanisms underlying toxicity induced by CdTe quantum dots determined in an invertebrate model organism. *Biomaterials*, 33, 1991-2000.
- Ambrosone, A., Roopin, M., Pelaz, B., Abdelmonem, A. M., Ackermann, L. M., Mattera, L., Allocca, M., Tino, A., Klapper, M., Parak, W. J., Levy, O. & Tortiglione, C. 2017. Dissecting common and divergent molecular pathways elicited by CdSe/ZnS quantum dots in freshwater and marine sentinel invertebrates. *Nanotoxicology*, 11, 289-303.
- Ambrosone, A. & Tortiglione, C. 2013. Methodological approaches for nanotoxicology using cnidarian models. *Toxicology mechanisms and methods*, 23, 207-216.
- Benseny-Cases, N., Klementieva, O., Cotte, M., Ferrer, I. & Cladera, J. 2014. Microspectroscopy (muFTIR) reveals co-localization of lipid oxidation and amyloid plaques in human Alzheimer disease brains. *Anal Chem*, 86, 12047-54.
- Bode, H. R. 2003. Head regeneration in Hydra. *Dev Dyn*, 226, 225-36.
- Cicatiello, P., Dardano, P., Pirozzi, M., Gravagnuolo, A. M., De Stefano, L. & Giardina, P. 2017. Self-assembly of two hydrophobins from marine fungi affected by interaction with surfaces. *Biotechnol Bioeng*, 114, 2173-2186.
- David, C. N. 1973. A quantitative method for maceration of Hydra tissue, Wilhelm Roux Arch. EntwMech. Org.
- Galliot, B., Miljkovic-Licina, M., De Rosa, R. & Chera, S. 2006. Hydra, a niche for cell and developmental plasticity. *Semin Cell Dev Biol*, 17, 492-502.
- Holstein, T. W., Hobmayer, E. & Technau, U. 2003. Cnidarians: an evolutionarily conserved model system for regeneration? *Dev Dyn*, 226, 257-67.
- Kao, S. H., Wang, W. L., Chen, C. Y., Chang, Y. L., Wu, Y. Y., Wang, Y. T., Wang, S. P., Nesvizhskii, A. I., Chen, Y. J., Hong, T. M. & Yang, P. C. 2015. Analysis of Protein Stability by the Cycloheximide Chase Assay. *Bio Protoc*, 5.
- Karntanut, W. & Pascoe, D. 2002. The toxicity of copper, cadmium and zinc to four different Hydra (Cnidaria : Hydrozoa). *Chemosphere*, 47, 1059-1064.

- Kovtun, A., Jones, D., Dell'elce, S., Treossi, E., Liscio, A., Palermo, V. 2019. Accurate chemical analysis of oxygenated graphene-based materials using X-ray photoelectron spectroscopy. *Carbon*, 143, 268-275.
- Murphy, M. E. 2013. The HSP70 family and cancer. *Carcinogenesis*, 34, 1181-8.
- Obrig, T. G., Culp, W.J., Mckeehan, W.L., Hardesty, B. 1971. The mechanism by which cycloheximide and related glutarimide antibiotics inhibit peptide synthesis on reticulocyte ribosomes. *J Biol Chem.* ;246(1):174-81., 246, 174-181.
- Oliviero, G., D'errico, S., Pinto, B., Nici, F., Dardano, P., Rea, I., De Stefano, L., Mayol, L., Piccialli, G. & Borbone, N. 2017. Self-Assembly of G-Rich Oligonucleotides Incorporating a 3'-3' Inversion of Polarity Site: A New Route Towards G-Wire DNA Nanostructures. *ChemistryOpen*, 6, 599-605.
- Palama, I., Di Maria, F., Viola, I., Fabiano, E., Gigli, G., Bettini, C. & Barbarella, G. 2011. Live-Cell-Permeant Thiophene Fluorophores and Cell-Mediated Formation of Fluorescent Fibrils. *Journal of the American Chemical Society*, 133, 17777-17785.
- Viola, I., Palama, I. E., Coluccia, A. M. L., Biasiucci, M., Dozza, B., Lucarelli, E., Di Maria, F., Barbarella, G. & Gigli, G. 2013. Physiological formation of fluorescent and conductive protein microfibers in live fibroblasts upon spontaneous uptake of biocompatible fluorophores. *Integrative Biology*, 5, 1057-1066.
- Wilby, O. K. & Tesh, J. M. 1990. The Hydra assay as an early screen for teratogenic potential. *Toxicol In Vitro*, 4, 582-3.